Washington University School of Medicine
Digital Commons@Becker

Open Access Publications

2019

NIX-mediated mitophagy promotes effector memory formation in antigen-specific CD8+ T cells

Shubhranshu S. Gupta

Robert Sharp

Colby Hofferek

Le Kuai

Gerald W. Dorn II

See next page for additional authors

Follow this and additional works at: https://digitalcommons.wustl.edu/open_access_pubs

Authors
Shubhranshu S. Gupta, Robert Sharp, Colby Hofferek, Le Kuai, Gerald W. Dorn II, Jin Wang, and Min Chen

Article

Cell Reports

NIX-Mediated Mitophagy Promotes Effector Memory Formation in Antigen-Specific CD8$^+$ T Cells

Graphical Abstract

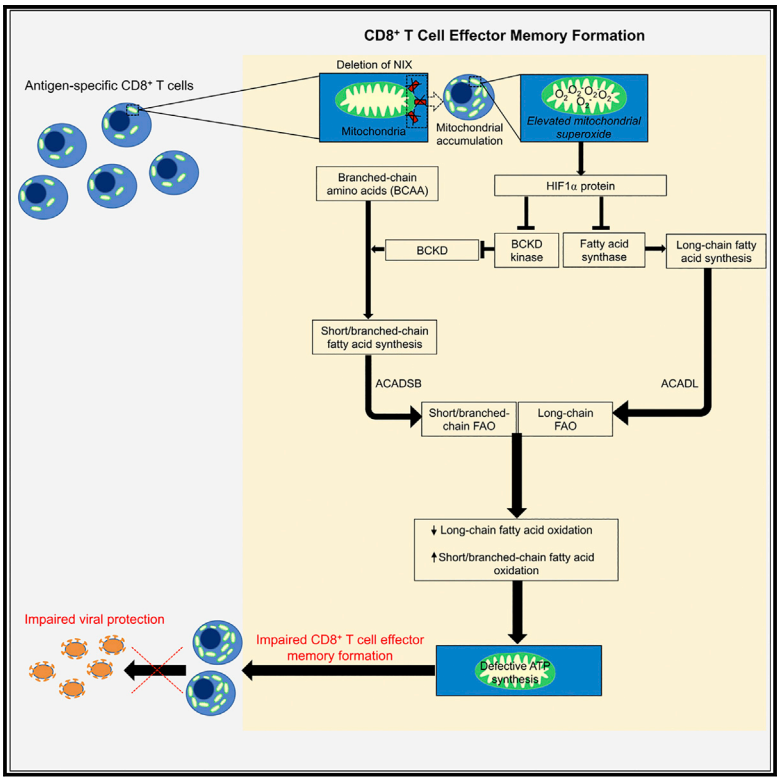

Highlights

- NIX regulates mitophagy during effector memory formation in CD8$^+$ T cells
- NIX-mediated mitophagy prevents HIF1α accumulation during contraction phase
- HIF1α alters metabolism from long-chain to short/branched-chain fatty acid oxidation
- Optimal ATP generation is critical for effector memory formation in CD8$^+$ T cells

Authors

Shubhranshu S. Gupta, Robert Sharp, Colby Hofferek, Le Kuai, Gerald W. Dorn II, Jin Wang, Min Chen

Correspondence

minc@bcm.edu

In Brief

Gupta et al. demonstrate that mitophagy mediated by NIX, a mitochondrial outer membrane protein, plays a critical role in CD8$^+$ T cell effector memory formation by regulating mitochondrial superoxide-dependent HIF1α protein accumulation and fatty acid metabolism. These findings elucidate the molecular mechanisms regulating T cell effector memory formation against viruses.

Gupta et al., 2019, Cell Reports *29*, 1862–1877
November 12, 2019 © 2019 The Authors.
https://doi.org/10.1016/j.celrep.2019.10.032

OPEN ACCESS
CellPress

Cell Reports
Article

NIX-Mediated Mitophagy Promotes Effector Memory Formation in Antigen-Specific CD8$^+$ T Cells

Shubhranshu S. Gupta,[1,2] Robert Sharp,[1] Colby Hofferek,[1] Le Kuai,[1] Gerald W. Dorn II,[3] Jin Wang,[4,5] and Min Chen[1,2,6,*]
[1]Department of Pathology and Immunology, Baylor College of Medicine, Houston, TX 77030, USA
[2]Interdepartmental Graduate Program in Translational Biology and Molecular Medicine, Baylor College of Medicine, Houston, TX 77030, USA
[3]Center for Pharmacogenomics, Department of Internal Medicine, Washington University School of Medicine, St. Louis, MO, USA
[4]Immunobiology and Transplant Science Center, Houston Methodist Research Institute, Houston, TX 77030, USA
[5]Department of Surgery, Weill Cornell Medical College, Cornell University, New York, NY 10065, USA
[6]Lead Contact
*Correspondence: minc@bcm.edu
https://doi.org/10.1016/j.celrep.2019.10.032

SUMMARY

Autophagy plays a critical role in the maintenance of immunological memory. However, the molecular mechanisms involved in autophagy-regulated effector memory formation in CD8$^+$ T cells remain unclear. Here we show that deficiency in NIX-dependent mitophagy leads to metabolic defects in effector memory T cells. Deletion of NIX caused HIF1α accumulation and altered cellular metabolism from long-chain fatty acid to short/branched-chain fatty acid oxidation, thereby compromising ATP synthesis during effector memory formation. Preventing HIF1α accumulation restored long-chain fatty acid metabolism and effector memory formation in antigen-specific CD8$^+$ T cells. Our study suggests that NIX-mediated mitophagy is critical for effector memory formation in T cells.

INTRODUCTION

Exposure to pathogens leads to activation of naive CD8$^+$ T cells, which then undergo clonal expansion. After clearance of infections, most of the antigen-specific CD8$^+$ T cells undergo apoptosis during contraction (effector-to-memory transition) phase (Kaech and Cui, 2012; Porter and Harty, 2006; Weant et al., 2008). However, some antigen-specific CD8$^+$ T cells survive and differentiate into memory CD8$^+$ T cells, which are metabolically quiescent. Memory CD8$^+$ T cells, which include both effector memory and central memory T cells, are formed in the secondary lymphoid organs such as spleen and lymph nodes (Kaech and Ahmed, 2001). Upon re-activation, effector memory CD8$^+$ T cells can rapidly expand into effector CD8$^+$ T cells and mount potent cytotoxic functions (Sallusto et al., 1999; Masopust et al., 2001). However, the processes that specifically regulate differentiation of effector memory CD8$^+$ T cells remain unclear.

Whereas activated effector CD8$^+$ T cells depend on glycolysis for their metabolic needs (Beckermann et al., 2017), memory CD8$^+$ T cells use long-chain fatty acid oxidation to generate energy (O'Sullivan et al., 2014). Fatty acid metabolism takes place in mitochondria, where they undergo β-oxidation to generate energy in the form of ATP. However, the molecules that regulate long-chain fatty acid oxidation in memory CD8$^+$ T cells have not been identified.

We and others have shown that deletion of NIX, a Bcl-2-family protein on the mitochondrial outer membrane (Matsushima et al., 1998), impairs the ability of autophagosomes to degrade mitochondria in reticulocytes via mitophagy (Sandoval et al., 2008; Schweers et al., 2007). Failure to clear dysfunctional mitochondria in the absence of NIX leads to accumulation of mitochondrial superoxide in natural killer (NK) memory cells (O'Sullivan et al., 2015). We have previously shown that mitochondrial superoxide is detrimental to immunological memory in B cells (Chen et al., 2014). The extent of superoxide production depends on mitochondrial quality regulated by mitophagy, wherein dysfunctional mitochondria are degraded via the autophagolysosomal pathway. Degraded mitochondria are later replaced by new functional mitochondria through mitochondrial biogenesis, which is regulated by mitochondrial transcription factor A (TFAM) (Araujo et al., 2018; Jornayvaz and Shulman, 2010; van der Windt et al., 2012). Although we and others have previously shown that autophagy is critical for formation and survival of memory B and T cells in mice (Chen et al., 2014, 2015; Murera et al., 2018; Puleston et al., 2014; Xu et al., 2014), the molecular mechanisms regulating formation of effector memory in CD8$^+$ T cells remain unknown.

In this study, using a T cell-specific NIX-deficient mouse model, we show that NIX-dependent mitophagy plays a protective role in differentiation of virus-specific effector memory CD8$^+$ T cells by modulating long-chain and short/branched-chain fatty acid oxidation.

RESULTS

NIX Is Critical for Formation of Effector Memory in Ova-Specific CD8$^+$ T Cells

To explore the role of NIX in effector memory CD8$^+$ T cell differentiation, we quantified *Nix* expression in CD8$^+$ T cells after

 © 2019 The Authors.
This is an open access article under the CC BY-NC-ND license (http://creativecommons.org/licenses/by-nc-nd/4.0/).

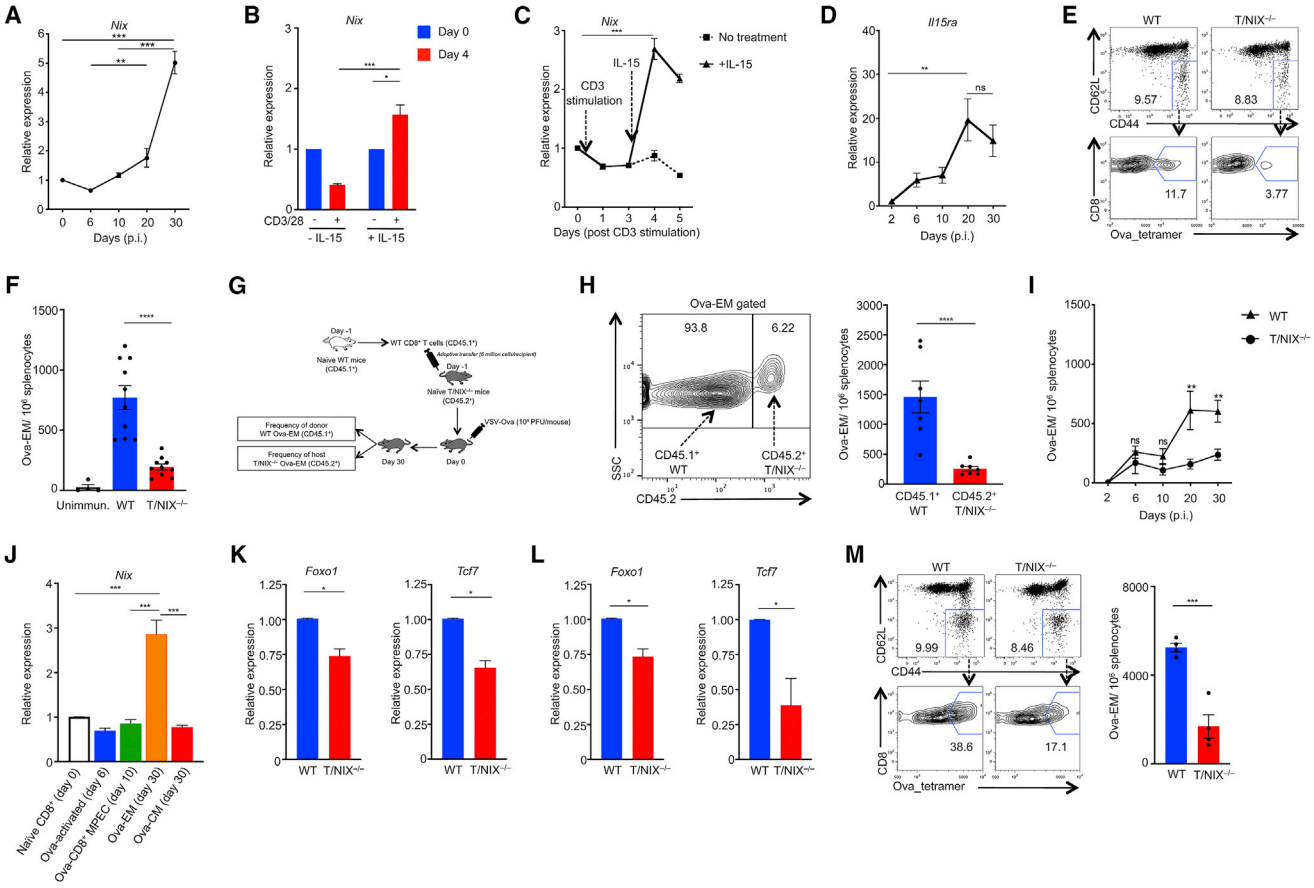

Figure 1. NIX Is Critical for Formation of Effector Memory in Ova-Specific CD8$^+$ T Cells

Spleens from OT-I mice (A–D) or wild-type (WT) and T/NIX$^{-/-}$ mice (E–K) were collected at designated time points.

(A) Kinetics of *Nix* expression in Ova-specific CD8$^+$ T cells (Ova-CD8$^+$) after VSV-Ova immunization.

(B) Gene expression of *Nix* in Ova-CD8$^+$ 24 h after addition of IL-15. CD8$^+$ T cells from naive OT-I mice were activated with anti-CD3 and anti-CD28 for 72 h, followed by IL-15 addition.

(C) Kinetics of *Nix* expression in Ova-CD8$^+$ after CD3-stimulation, followed by IL-15 addition.

(D) Kinetics of *Il15ra* expression in Ova-CD8$^+$ after VSV-Ova immunization. Ova-CD8$^+$ from mice within the same experimental group in (A)–(D) were pooled before analysis.

(E) Representative dot plot showing percentage of Ova-EM in WT or T/NIX$^{-/-}$ spleens on day 30 p.i. with 10^4 plaque-forming units (PFU) of VSV-Ova.

(F) Mean frequencies of Ova-EM from (E).

(G) Experimental model for adoptive transfer experiment performed in (H).

(H) Left: representative plot showing percentages of CD45.1$^+$ WT and CD45.2$^+$ T/NIX$^{-/-}$ Ova-EM in CD45.2$^+$ T/NIX$^{-/-}$ mice 30 days after VSV-Ova immunization. Right: mean frequencies of CD45.1$^+$ WT and CD45.2$^+$ T/NIX$^{-/-}$ Ova-EM from experiment performed in the left panel.

(I) Kinetics of effector memory formation in Ova-CD8$^+$ *in vivo* in WT or T/NIX$^{-/-}$ mice after VSV-Ova immunization.

(J) Gene expression of *Nix* in day 0 naive, day 6 Ova-activated, day 10 Ova-CD8$^+$ MPECs, day 30 Ova-EM, and day 30 Ova-CM in WT mice after VSV-Ova immunization.

(K and L) Gene expression of *Foxo1* (left panel) and *Tcf7* (right panel) in day 10 Ova-CD8$^+$ MPECs (K) or day 30 Ova-EM (L) harvested from WT or T/NIX$^{-/-}$ spleens after VSV-Ova immunization.

(M) *In vitro* differentiation of Ova-EM. Left: representative plot for percentage of WT or T/NIX$^{-/-}$ Ova-EM on day 8. Right: mean frequency of Ova-EM from left panel.

In (E) and (M), CD8$^+$Ova_tetramer$^+$ population (Ova-EM) was gated on CD3$^+$CD8$^+$CD43$^-$CD62L$^-$CD44$^+$ population. Data are representative of two or more independent experiments (n = 3–10). Data were analyzed using one-way ANOVA with Bonferroni's posttest (mean ± SEM) in (A)–(D); two-tailed Student's t test (mean ± SEM) in (F), (H, right), (J)–(L), and (M, right); and two-way ANOVA with Bonferroni's posttests (mean ± SEM) in (I). *$p < 0.05$, **$p < 0.01$, ***$p < 0.001$, and ****$p < 0.0001$. See also Figures S1 and S2.

immunization of wild-type (WT) mice with vesicular stomatitis virus co-expressing ovalbumin (VSV-Ova). While *Nix* was downregulated in Ova-specific CD8$^+$ T cells during primary response on day 6 post-immunization (p.i.), it was upregulated from day 10 p.i. (Figure 1A), the onset of contraction phase (effector-to-memory transition phase) in CD8$^+$ T cells (Xu et al., 2014). The expression of *Nix* continued to further increase during the course of immunological memory formation in Ova-specific CD8$^+$ T cells

(Figure 1A), suggesting that NIX potentially plays a role in CD8$^+$ T cell memory formation.

IL-15 plays a critical role in immunological memory formation (Sato et al., 2007; Xu et al., 2016), but its mechanism is unclear. We found that *Nix* expression was upregulated in Ova-specific CD8$^+$ T cells within 24 h of IL-15 addition (Figure 1B). We further examined whether the initial downregulation in *Nix* expression during primary response (Figure 1A) was mediated through TCR signaling. Upon CD3 stimulation, Ova-specific CD8$^+$ T cells downregulated *Nix*; however, *Nix* expression was upregulated after subsequent addition of IL-15 (Figure 1C). Consistent with increased *Nix* expression during the contraction phase (Figure 1A), we observed concomitant increase in IL-15 receptor α (*Il15ra*) expression in Ova-specific CD8$^+$ T cells during the contraction phase in VSV-Ova-immunized WT mice (Figure 1D). These data suggest that TCR signaling downregulates *Nix* expression during the primary response, while IL-15 signaling might contribute to the upregulation of *Nix* expression during memory formation in antigen-specific CD8$^+$ T cells.

To investigate the role of NIX in immunological memory formation, we generated mice with T cell-specific deletion of *Nix* (*Lck*^{cre} × *Nix*$^{f/f}$ mice, denoted T/NIX$^{-/-}$). The development of double-negative (DN; CD44$^-$CD25$^-$) or double-positive (DP; CD44$^+$CD25$^+$) T cell populations were similar between WT and T/NIX$^{-/-}$ mice (Figures S1A and S1B). Within the DN population, DN1 (CD44$^+$CD25$^-$), DN2 (CD44$^+$CD25$^+$), DN3 (CD44$^-$CD25$^+$), and DN4 (CD44$^-$CD25$^-$) cells were also similar between WT and T/NIX$^{-/-}$ mice (Figures S1C and S1D). Frequency of mature CD4$^+$ and CD8$^+$ T cells, naive, central memory and effector CD8$^+$ T cells were also comparable between the WT and T/NIX$^{-/-}$ mice (Figures S1E–S1H). These data suggest that NIX deficiency in T cells did not alter T cell development and migration to periphery.

CD43 (1B11) is expressed on activated but not memory CD8$^+$ T cells (Harrington et al., 2000; Hikono et al., 2007; Olson et al., 2013). Therefore, we used CD3$^+$CD8$^+$CD62L$^-$CD44$^+$CD43$^-$Ova_tetramer$^+$ cells as Ova-specific effector memory CD8$^+$ T cells (Ova-EM), CD3$^+$CD8$^+$CD62L$^+$CD44$^+$CD43$^-$Ova_tetramer$^+$ cells as Ova-specific central memory CD8$^+$ T cells (Ova-CM), and CD3$^+$CD8$^+$CD62L$^-$CD44$^+$CD43$^+$Ova_tetramer$^+$ cells as Ova-specific activated CD8$^+$ T cells (Ova-activated) in our experiments. In addition, we used CD3$^+$CD8$^+$CD62L$^-$CD44$^+$CD127$^+$Ova_tetramer$^+$ cells on day 10 p.i. as Ova-specific CD8$^+$ memory precursor effector cells (Ova-CD8$^+$ MPECs); which exhibited no significant alteration in their expression of KLRG1, a marker of terminal differentiation (Joshi et al., 2007; Voehringer et al., 2002; Yuzefpolskiy et al., 2015), between WT and T/NIX$^{-/-}$ mice (Figure S2A).

We next immunized WT and T/NIX$^{-/-}$ mice with VSV-Ova, which was cleared by both the hosts before the contraction phase (Figure S2B), and measured the frequency of Ova-EM and Ova-CM 30 days p.i. Interestingly, we observed significantly reduced frequency of Ova-EM in T/NIX$^{-/-}$ mice (Figures 1E and 1F) but not Ova-CM (Figure S2C). When additional T cell memory phenotypic markers, KLRG1 and CD127 (Bengsch et al., 2007; Joshi et al., 2007), were included, CD127$^+$KLRG1$^-$ Ova-EM was also impaired in T/NIX$^{-/-}$ mice (Figures S2D and S2E). Some studies suggest that T cell memory is promoted by CXCR5 and TCF7 but inhibited by TIM3 (Avery et al., 2018; Billingsley et al., 2015; Leong et al., 2016; Sabins et al., 2017; Yu and Ye, 2018). We found that CXCR5$^+$TIM3$^-$TCF7$^+$ Ova-EM cells were significantly impaired in T/NIX$^{-/-}$ mice 30 days p.i. (Figures S2F and S2G). To test if this impairment was CD8$^+$ T cell intrinsic, we adoptively transferred CD8$^+$ T cells using the experimental setup as described (Figure 1G). We found that the formation of effector memory was defective in host CD45.2$^+$ T/NIX$^{-/-}$ CD8$^+$ T cells compared with donor CD45.1$^+$ WT CD8$^+$ T cells (Figure 1H), suggesting that the impairment in CD8$^+$ T cell effector memory formation due to NIX ablation was intrinsic in nature. Moreover, frequency of Ova-activated CD8$^+$ T cells did not change in T/NIX$^{-/-}$ mice during the peak primary response (D'Souza and Hedrick, 2006; Figure S2H), and CD8$^+$ T cells from naive WT and T/NIX$^{-/-}$ mice proliferated to the same extent upon CD3/CD28 stimulation (Figure S2I), suggesting that reduced Ova-EM frequency was not due to altered primary response. Furthermore, BNIP3, a NIX homolog, was not required for effector memory formation in Ova-specific CD8$^+$ T cells (Figures S2J and S2K), although there was an overall reduction in *Bnip3* expression in Ova-specific CD8$^+$ T cells during VSV-Ova infection (Figure S2L), likely due to *Bnip3* downregulation during central memory formation (Figure S2M). Pink1 and Parkin (Park2), which also control mitophagy in mammalian cells (Gkikas et al., 2018; Jin and Youle, 2012), were not significantly upregulated during T cell memory formation either (Figure S2N). These data suggest a unique role for NIX in CD8$^+$ T cell effector memory formation.

Next, we found that CD8$^+$ T cell effector memory formation was impaired between days 10 and 20 p.i. in T/NIX$^{-/-}$ mice (Figures 1I and S2O), suggesting that NIX deficiency during the contraction phase was the causative factor. Caspase-3 (*Casp3*) can mediate apoptosis in virus-specific effector T cells during the contraction phase (Garrod et al., 2012; Kapoor et al., 2014; Sabbagh et al., 2004; Secinaro et al., 2018). We found that *Casp3* expression was increased in T/NIX$^{-/-}$ Ova-CD8$^+$ MPECs but not in fully formed T/NIX$^{-/-}$ Ova-EM (Figure S2P). Moreover, apoptosis during the contraction phase was increased in T/NIX$^{-/-}$ Ova-CD8$^+$ MPECs but not Ova-EM, as indicated by annexin V staining (Figures S2Q and S2R). These data suggest that the defective CD8$^+$ T cell effector memory formation in T/NIX$^{-/-}$ mice was caused by a loss of Ova-CD8$^+$ MPECs but not due to an increased apoptosis in newly formed Ova-EM. This critical requirement of NIX during the contraction phase was consistent with *Nix* upregulation in Ova-CD8$^+$ MPECs on day 10 p.i., followed by a significant upregulation in Ova-EM by day 30 p.i. in WT mice (Figure 1J). In contrast to Ova-EM, NIX expression did not change in Ova-CM, consistent with no change in Ova-CM differentiation despite absence of NIX (Figure S2C). We also quantified expression of *Foxo1* and *Tcf7*, transcription factors critical for CD8$^+$ T cell memory formation (Lin et al., 2016; Zhou and Xue, 2012; Hess Michelini et al., 2013), in Ova-CD8$^+$ MPECs (Danilo et al., 2018; Kim et al., 2013). Their expression was significantly reduced in T/NIX$^{-/-}$ Ova-CD8$^+$ MPECs (Figure 1K). In addition, expression of *Blimp-1*, a transcription factor inhibiting CD8$^+$ T cell memory formation (Rutishauser et al., 2009), was upregulated in T/NIX$^{-/-}$ Ova-CD8$^+$ MPECs (Figure S2S). Likewise, *Foxo1* and *Tcf7* were significantly

reduced (Figure 1L) and *Blimp-1* was upregulated (Figure S2T) in T/NIX$^{-/-}$ Ova-EM 30 days p.i. We also studied formation of Ova-EM *in vitro* in the presence of IL-15 (Buck et al., 2016; O'Sullivan et al., 2014; van der Windt et al., 2012, 2013), with effector-to-memory transition phase falling between day 3 and day 7 post-activation (Figure S2U), and confirmed that the absence of NIX significantly impaired Ova-EM formation (Figure 1M). Together, our data suggest that NIX is critical for optimal generation of effector memory in antigen-specific CD8$^+$ T cells during the contraction phase.

Impaired Effector Memory Formation in Antigen-Specific CD8$^+$ T Cells Leads to a Defective Recall Response

We next transferred equal numbers of CD45.2$^+$ Ova-EM (from WT or T/NIX$^{-/-}$ mice) into naive CD45.1$^+$ hosts, which were subsequently challenged with VSV-Ova. Forty-eight hours later, memory recall response of CD45.2$^+$ Ova-EM was studied (Chen et al., 2006; D'Souza and Hedrick, 2006). Upon re-activation of Ova-EM by VSV-Ova, *Nix* expression was downregulated in CD45.2$^+$ WT CD8$^+$ T cells (Figure S3A), consistent with our earlier data (Figures 1A, 1C, and 1J) demonstrating that CD8$^+$ T cell activation downregulates *Nix* expression. We then investigated if limited effector memory formation in T/NIX$^{-/-}$ CD8$^+$ T cells would cause a defective memory recall response. Recipients of *in vivo* generated T/NIX$^{-/-}$ Ova-EM showed a reduced recall response (Figure 2A), which was verified by ELISA (Figure 2B) and intracellular staining (Figures 2C, 2D, and S3B) for IFN-γ and IL-2. In addition, T/NIX$^{-/-}$ Ova-EM proliferated significantly lesser than their WT counterparts upon VSV-Ova re-challenge (Figure 2E). Consistent with defective memory recall response in Ova-EM developed *in vivo*, we also observed an impaired memory recall response by T/NIX$^{-/-}$ Ova-EM generated *in vitro* (Figures 2F–2I and S3C). Proliferation upon secondary challenge has been shown to depend on mitochondrial spare respiratory capacity (SRC) in memory T cells (van der Windt et al., 2013). Hence, we performed extracellular flux analysis (Seahorse assay) to measure mitochondrial SRC and found that T/NIX$^{-/-}$ Ova-EM had significantly lesser SRC (Figures S3D and S3E). These data indicate that defective effector memory formation in antigen-specific T/NIX$^{-/-}$ CD8$^+$ T cells resulted in a defective recall response, likely through impairment in mitochondrial SRC.

Absence of NIX Causes Mitochondrial Accumulation during Effector Memory Formation in Antigen-Specific CD8$^+$ T Cells

We next examined the molecular mechanism behind impaired CD8$^+$ T cell effector memory formation in T/NIX$^{-/-}$ mice. Because NIX is involved in mitochondrial clearance in red blood cells (Sandoval et al., 2008; Schweers et al., 2007), we quantified total mitochondria in Ova-EM formed *in vivo* after VSV-Ova immunization. T/NIX$^{-/-}$ Ova-EM showed significantly more mitochondria than WT controls on day 30 p.i. (Figure 3A), which we verified via immunostaining of mitochondrial COX IV (Figures 3B and 3C). Mitochondrial levels in naive CD8$^+$ T cells were comparable between WT and T/NIX$^{-/-}$ mice (Figures S4A–S4D), suggesting that mitochondrial accumulation due to deletion of NIX occurred during effector memory formation, rather than naive CD8$^+$ T cell stage.

To determine if mitochondrial accumulation in T/NIX$^{-/-}$ Ova-EM occurred because of impaired mitophagy, we performed co-localization analysis of stained mitochondria and autophagosomes in Ova-EM generated *in vivo* on day 30 p.i. Mitophagy in Ova-EM was significantly decreased in T/NIX$^{-/-}$ mice (Figures 3D and S4E), but not because of altered basal autophagy, as shown by similar levels of LC3 and autophagic vacuoles in WT and T/NIX$^{-/-}$ Ova-EM (Figures S4F and S4G), suggesting that reduced mitophagy in T/NIX$^{-/-}$ Ova-EM stemmed from an inability of available autophagosomes to degrade mitochondria. Interestingly, there were no significant changes in the level of mitochondria (Figures S4A–S4D) and mitophagy (Figure S4E) in Ova-CM in absence of NIX. We also observed significantly higher levels of mitophagy in WT Ova-EM compared with WT naive CD8$^+$ T cells, which reversed upon deletion of NIX (Figure S4E). These data suggest that NIX regulates mitophagy during CD8$^+$ T cell effector memory formation, but not at naive CD8$^+$ T cell stage. As expected, deletion of NIX did not alter basal autophagy in naive CD8$^+$ T cells or Ova-EM, although Ova-EM showed significantly more basal autophagy than naive CD8$^+$ T cells (Figures S4F and S4G).

Mitochondrial accumulation in T/NIX$^{-/-}$ Ova-EM could also be due to increased mitochondrial biogenesis, which is regulated by TFAM (Araujo et al., 2018; Jornayvaz and Shulman, 2010; van der Windt et al., 2012) in mammalian cells. We found no significant difference in *Tfam* gene expression (Figure 3E) or TFAM protein level (Figure 3F) between WT and T/NIX$^{-/-}$ mice, indicating that mitochondrial biogenesis did not play a role in mitochondrial accumulation in T/NIX$^{-/-}$ Ova-EM.

Deletion of NIX Results in Elevation of Mitochondrial Superoxide, Thereby Impairing CD8$^+$ T Cell Effector Memory Formation during Contraction Phase

Accumulation of mitochondria in immune cells has been shown to elevate mitochondrial superoxide (Chen et al., 2014; O'Sullivan et al., 2015). Hence, we stained Ova-specific CD8$^+$ T cells with MitoSOX Red during the contraction phase and found significantly higher mitochondrial superoxide in T/NIX$^{-/-}$ mice (Figures 4A, 4B, S5A, and S5B). Because mitochondrial superoxide induces mitophagy of dysfunctional mitochondria so as to mitigate mitochondrial stress (Bordi et al., 2017; Ježek et al., 2018; Shefa et al., 2019), we hypothesized that elevation of mitochondrial superoxide in absence of NIX-mediated mitophagy would exacerbate mitochondrial stress in antigen-specific CD8$^+$ T cells. Indeed, we found that mitochondrial stress in T/NIX$^{-/-}$ Ova-specific CD8$^+$ T cells was significantly higher during the contraction phase, as indicated by increased mitochondrial membrane depolarization (Chirichigno et al., 2002; Herst et al., 2017; Witte and Horke, 2011; Figures 4C and 4D) and mtDNA damage (Herst et al., 2017; Kang and Hamasaki, 2003; Figure S5C). This suggests that deletion of NIX caused an elevation of superoxide in the accumulated mitochondria of virus-specific CD8$^+$ T cells during contraction phase, and this likely increased mitochondrial stress during effector-to-memory transition.

We next asked whether this increase in mitochondrial superoxide during contraction phase was responsible for defective

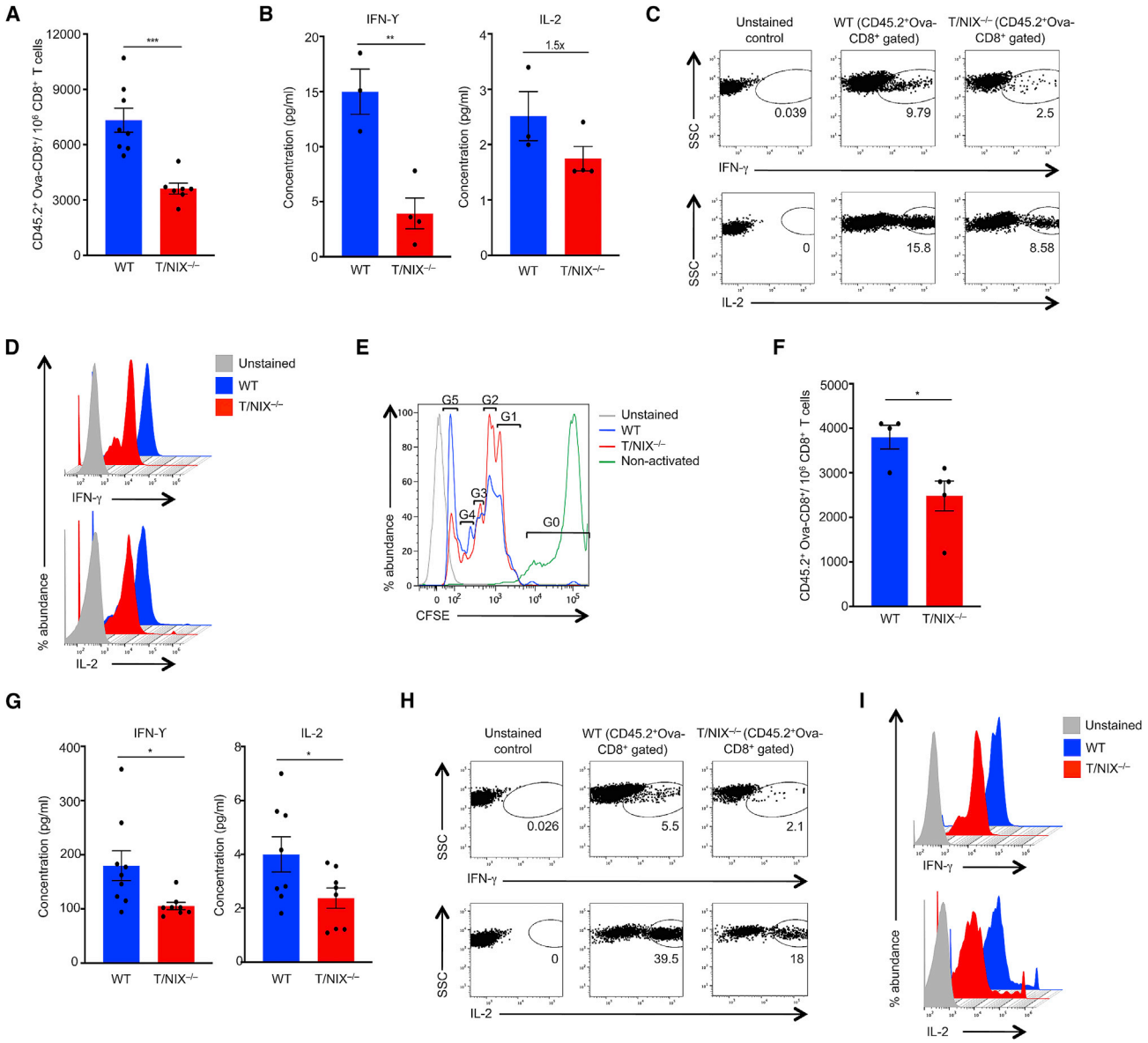

Figure 2. Deletion of NIX Leads to an Impaired Memory Recall in Ova-Specific Effector Memory CD8+ T Cells

Ova-EM formed *in vivo* (A–E) or *in vitro* (F–I) from CD45.2+ WT or T/NIX−/− mice were adoptively transferred into naive CD45.1+ mice. CD45.1+ hosts were challenged with 10^4 PFU of VSV-Ova 24 h later. Forty-eight hours later, spleen and serum were harvested for analyses.

(A) CD45.2+ Ova-CD8+ in CD45.1+ recipients receiving *in vivo* generated CD45.2+ WT or T/NIX−/− Ova-EM.

(B) Serum IFN-γ (left) and IL-2 (right) in CD45.1+ recipients from (A).

(C) Plot showing IFN- γ and IL-2 producing CD45.2+ Ova-CD8+ in CD45.1+ recipients receiving *in vivo* generated CD45.2+ WT or T/NIX−/− Ova-EM.

(D) Intracellular IFN-γ and IL-2 in CD45.2+ Ova-CD8+ in CD45.1+ recipients receiving CD45.2+ WT or T/NIX−/− Ova-EM. Geometric mean fluorescence index (MFI) values for IFN-γ were 2,292 ± 130.1 (WT) and 1,831 ± 143.6 (T/NIX−/−). Geometric MFIs for IL-2 were 1,126 ± 88.91 (WT) and 920.7 ± 166.3 (T/NIX−/−).

(E) *In vivo* proliferation of re-activated WT or T/NIX−/− Ova-EM measured by CFSE staining. Peaks corresponding to G1, G2, G3, G4, and G5 represent the generations of cells after successive cell division cycles. Proliferation index: 1.611 ± 0.023 (WT) and 1.454 ± 0.026 (T/NIX−/−) ($p < 0.001$).

(F) CD45.2+ Ova-CD8+ in CD45.1+ recipients receiving *in vitro* generated CD45.2+ WT or T/NIX−/− Ova-EM.

(G) Serum IFN-γ and IL-2 in CD45.1+ recipients from (F).

(H) Plot showing frequencies of IFN-γ- and IL-2-producing CD45.2+ Ova-CD8+ in CD45.1+ recipients receiving *in vitro* generated CD45.2+ WT or T/NIX−/− Ova-EM.

(I) Intracellular IFN-γ and IL-2 in CD45.2+ Ova-CD8+ in CD45.1+ recipients receiving *in vitro* generated CD45.2+ WT or T/NIX−/− Ova-EM. Geometric MFIs for IFN-γ were 7,120 ± 503.1 (WT) and 5,363 ± 551.3 (T/NIX−/−). Geometric MFIs for IL-2 were 5,154 ± 394.6 (WT) and 2,668 ± 489.4 (T/NIX−/−).

Data in (A), (B), and (E)–(G) are representative of two or more independent experiments (n = 3–9), and data in (C), (D), (H), and (I) are representative of three or four biological replicates per group. Data were analyzed using two-tailed Student's t test (mean ± SEM). *$p < 0.05$, **$p < 0.01$, and ***$p < 0.001$. See also Figure S3.

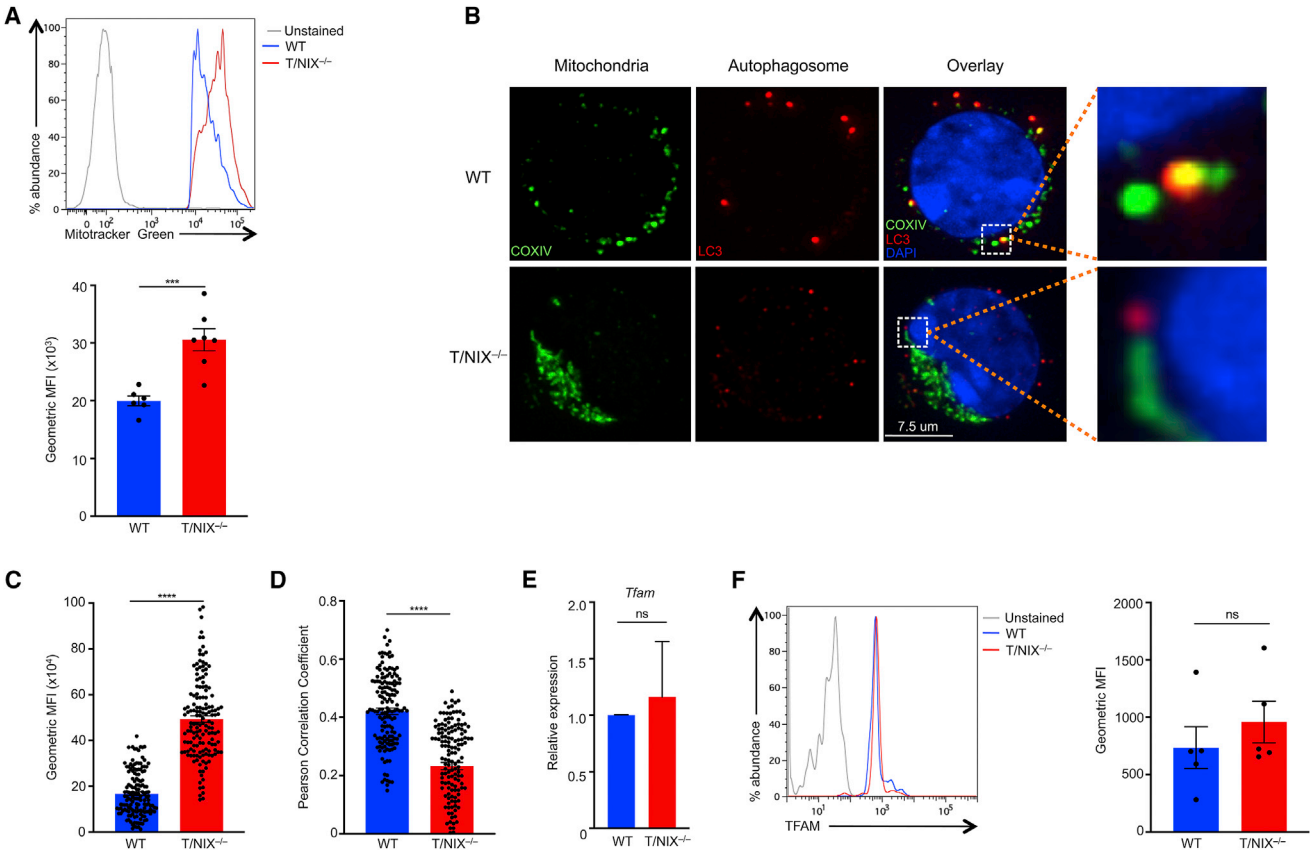

Figure 3. Deletion of NIX Leads to Mitochondrial Accumulation in Ova-Specific Effector Memory CD8$^+$ T Cells

Spleens from WT or T/NIX$^{-/-}$ mice were collected 30 days p.i. with VSV-Ova for analyses.

(A) Top: MitoTracker Green staining in Ova-EM. Bottom: geometric mean fluorescence index (MFI) of MitoTracker Green staining from top panel.

(B) Representative image of WT or T/NIX$^{-/-}$ Ova-EM stained with COX IV (mitochondria) and LC3 (autophagosomes) obtained by immunocytochemistry.

(C and D) Mitochondrial median fluorescence index (MFI) (C) and (D) co-localization analysis of mitochondria and autophagosomes in Ova-EM from (B). For each independent experiment in (B)–(D), Ova-EM were pooled from mice within the same experimental group, and 150 cells/group were imaged. Each point represents one Ova-EM.

(E) Gene expression of *Tfam* in Ova-EM. Ova-EM from mice within the same experimental group were pooled before analysis.

(F) Intracellular staining of TFAM in Ova-EM.

Data are representative of two or more independent experiments (n = 5–7). Data were analyzed using two-tailed Student's t test (mean ± SEM). **$p < 0.01$, ***$p < 0.001$, and ****$p < 0.0001$. ns, non-significant. See also Figure S4.

CD8$^+$ T cell effector memory formation in the absence of NIX. Because we observed that both impairment in effector memory formation and accumulation of mitochondrial superoxide occurred during contraction phase (days 10–20 p.i.), we chose day 13 p.i. as the time point for injecting N-acetyl cysteine (NAC), a scavenger of mitochondrial superoxide (Chen et al., 2014; O'Sullivan et al., 2015), into WT and T/NIX$^{-/-}$ mice. Administration of NAC restored effector memory formation in T/NIX$^{-/-}$ Ova-CD8$^+$ T cells both *in vivo* (Figures 4E and 4F) and *in vitro* (Figures 4G and 4H). Treatment of WT groups *in vivo* and *in vitro* with NAC did not significantly alter CD8$^+$ T cell effector memory formation, suggesting that over-accumulation of mitochondrial superoxide during contraction phase in T/NIX$^{-/-}$ mice contributed to impaired CD8$^+$ T cell effector memory formation. Furthermore, treatment with NAC rescued defective proliferation of T/NIX$^{-/-}$ Ova-EM during memory recall response (Figure S5D).

Mitochondrial Superoxide Elevates HIF1α during Contraction Phase in T/NIX$^{-/-}$ Mice

Mitochondrial superoxide increases expression of hypoxia-inducible factor 1 (HIF1α) in mammalian cells (Chandel et al., 1998, 2000), which is required for metabolism in activated CD8$^+$ T cells (Lee and Simon, 2012; Pollizzi and Powell, 2014; Menk et al., 2018). We therefore performed intracellular staining for HIF1α protein in Ova-EM generated *in vivo* 30 days after VSV-Ova immunization and found significantly elevated HIF1α in T/NIX$^{-/-}$ Ova-EM (Figures 5A, 5B, S5E, and S5F). Although WT Ova-CD8$^+$ downregulated HIF1α protein during transition from peak primary response (day 6 p.i.) to contraction phase (day 13 p.i.), HIF1α protein continued to stay elevated in T/NIX$^{-/-}$ Ova-CD8$^+$ even during the contraction phase (Figures 5C and 5D), suggesting that mitochondrial superoxide likely upregulated HIF1α during

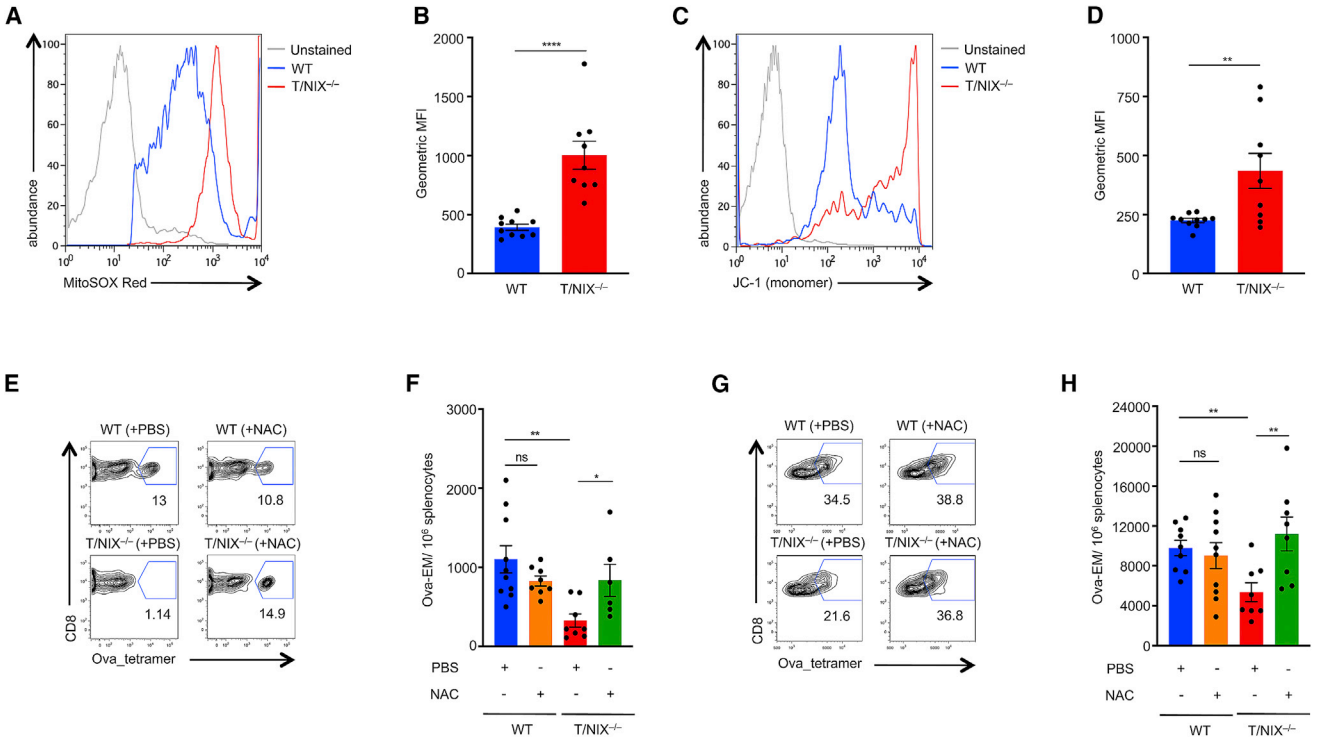

Figure 4. Deletion of NIX Results in Elevation of Mitochondrial Superoxide, Thereby Impairing CD8$^+$ T Cell Effector Memory Formation during Contraction Phase

Spleens from WT and T/NIX$^{-/-}$ mice were harvested on designated time points after immunization with 10^4 PFU VSV-Ova.

(A) MitoSOX Red staining in Ova-CD8$^+$ from WT and T/NIX$^{-/-}$ mice 20 days p.i.

(B) Geometric MFI for mitochondrial superoxide in Ova-CD8$^+$ from (A).

(C) Mitochondrial membrane depolarization (JC-1 monomer fluorescence) in Ova-CD8$^+$ from WT and T/NIX$^{-/-}$ mice 20 days p.i.

(D) Geometric MFI for JC-1 fluorescence in Ova-CD8$^+$ from (C).

(E) Representative plot showing percentage of Ova-EM 30 days p.i. in WT and T/NIX$^{-/-}$ mice that were treated with NAC or vehicle control (PBS) on days 13, 20, and 27 p.i.

(F) Mean frequencies of Ova-EM from (E).

(G) Representative plot showing percentage of WT and T/NIX$^{-/-}$ Ova-EM formed *in vitro*, after NAC or PBS treatment.

(H) Mean frequencies of Ova-EM from (G).

Data are representative of two or more independent experiments (n = 6–10). Data were analyzed using two-tailed Student's t test (mean ± SEM). *$p < 0.05$, **$p < 0.01$, and ****$p < 0.0001$. ns, non-significant. See also Figure S5.

effector-to-memory transition phase. Because HIF1α is upregulated in activated T cells (McNamee et al., 2013) expressing KLRG1 (Robbins et al., 2003; Tata and Brossay, 2018), it was also possible that elevation of HIF1α in T/NIX$^{-/-}$ antigen-specific CD8$^+$ T cells was a result of altered KLRG1 differentiation during contraction phase. However, we found that the upregulation of HIF1α occurred regardless of KLRG1 differentiation during effector memory formation in T/NIX$^{-/-}$ Ova-CD8$^+$ T cells (Figures S5G and S5H). We next measured intracellular HIF1α protein level in Ova-EM isolated from T/NIX$^{-/-}$ mice, which were treated with NAC during the contraction phase. Removal of mitochondrial superoxide by NAC treatment reversed HIF1α accumulation in T/NIX$^{-/-}$ Ova-EM (Figures 5E and 5F), supporting that HIF1α accumulation is a downstream effect of mitochondrial superoxide. These data suggest that increased mitochondrial superoxide during the contraction phase increased HIF1α level during CD8$^+$ T cell effector memory formation in T/NIX$^{-/-}$ mice.

Elevated HIF1α Alters Mitochondrial Fatty Acid Metabolism during CD8$^+$ T Cell Effector Memory Formation in T/NIX$^{-/-}$ Mice, Leading to Impairment in ATP Synthesis

We next investigated the mechanism through which HIF1α acts during effector memory formation in antigen-specific CD8$^+$ T cells. Chronic HIF1α expression in mammalian cells inhibits expression of fatty acid synthase (*Fasn*) (Qu et al., 2011). FASN participates in the synthesis of long-chain fatty acids, which memory CD8$^+$ T cells depend upon for their metabolism (O'Sullivan et al., 2014; Sugiura and Rathmell, 2018). In T/NIX$^{-/-}$ mice, we saw significantly decreased *Fasn* expression in Ova-EM (Figure 6A), indicating that T/NIX$^{-/-}$ Ova-CD8$^+$ likely funnel their bioenergetic activities through an alternative metabolic pathway during effector memory formation. Hence, we performed PCR array for T cell metabolic pathways (Almeida et al., 2016; Ganeshan and Chawla, 2014) and found significant upregulation in the expression of short/branched-chain specific acyl-CoA

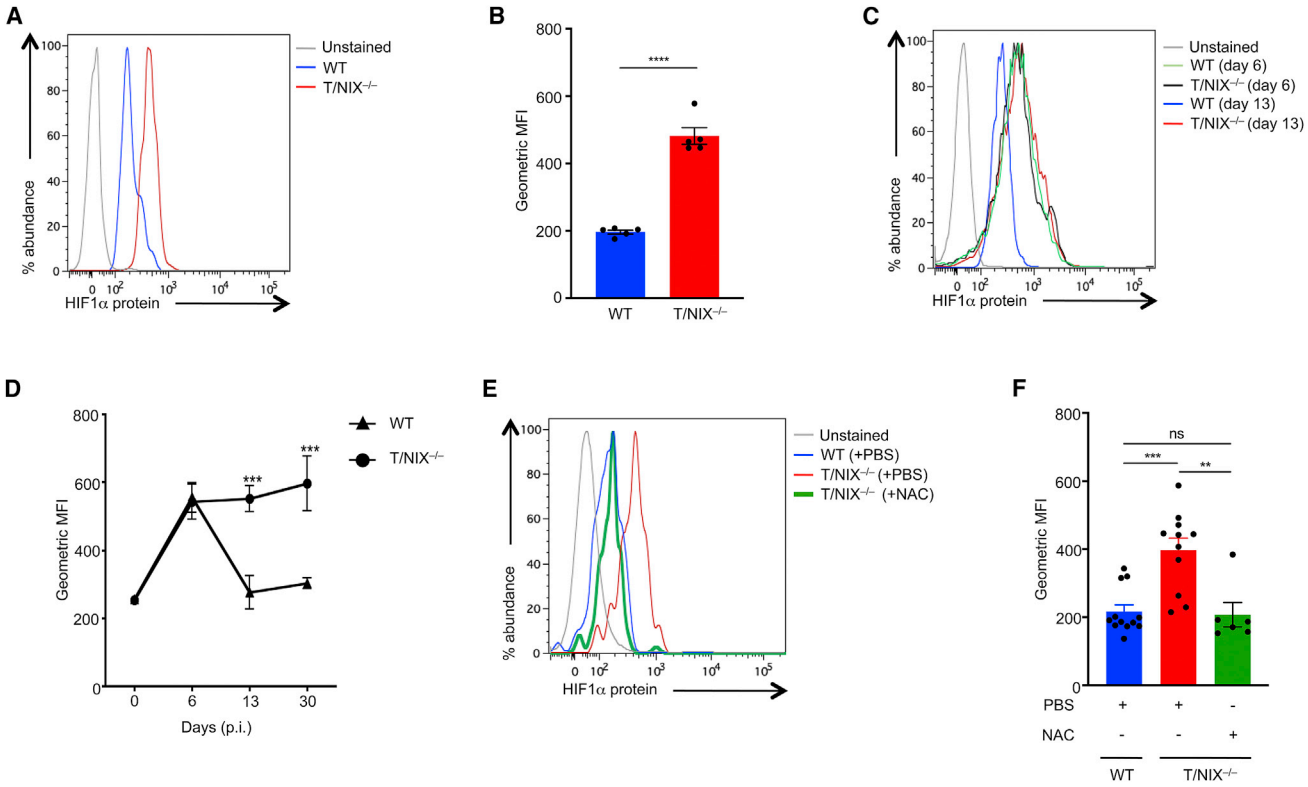

Figure 5. Mitochondrial Superoxide Elevates HIF1α during Contraction Phase in T/NIX$^{-/-}$ Mice

Spleens from WT or T/NIX$^{-/-}$ mice were collected at designated time points after immunization with 10^4 PFU VSV-Ova.

(A) Intracellular HIF1α protein level in Ova-EM 30 days p.i. in WT and T/NIX$^{-/-}$ mice.

(B) Geometric MFI of HIF1α protein staining from (A).

(C) Intracellular HIF1α protein level in Ova-specific effector CD8$^+$ T cells during peak primary response (day 6 p.i.) and contraction phase (day 13 p.i.) in WT and T/NIX$^{-/-}$ mice.

(D) Geometric MFI of HIF1α protein staining from (C).

(E) Intracellular HIF1α protein level in Ova-CD8$^+$ in NAC or PBS treated WT and T/NIX$^{-/-}$ mice.

(F) Geometric MFI of HIF1α protein staining from (E).

Data are representative of two or more independent experiments (n = 3–12). Data were analyzed using two-tailed Student's t test (mean ± SEM) in (B) and (F) and two-way ANOVA with Bonferroni's posttest (mean ± SEM) in (D). **p < 0.01, ***p < 0.001, and ****p < 0.0001. ns, non-significant. See also Figure S5.

dehydrogenase (*Acadsb*) in T/NIX$^{-/-}$ Ova-EM (Figure 6B). ACADSB contributes to oxidation of short/branched-chain fatty acids (Alfardan et al., 2010; Jiang et al., 2018; Luís et al., 2011; Vockley et al., 2000); thus, T/NIX$^{-/-}$ Ova-CD8$^+$ T cells likely exhibited a shift in fatty acid metabolism during effector memory formation. Consistent with reduced long-chain fatty acid synthesis, we observed a decrease in gene expression of long-chain acyl-CoA dehydrogenase (*Acadl*) (Figure 6B), as this enzyme carries out β-oxidation of long-chain fatty acids synthesized by FASN (Kurtz et al., 1998). Moreover, we noted no significant alteration in glycolysis, glutaminolysis, short/medium/very long chain fatty acid oxidation, or peroxisomal fatty acid oxidation (Figure 6B). A shift to short/branched-chain fatty acid oxidation was further verified in T/NIX$^{-/-}$ Ova-EM by decreased expression of branched-chain-α-keto acid dehydrogenase kinase (*Bckdk*) (Figure 6C), an enzyme that restricts synthesis of short/branched-chain fatty acids from branched-chain amino acids (BCAAs) (Harris et al., 1986; Shimomura et al., 2006). Consistently, upregulated short/branched-chain fatty acid metabolism resulted in an increased synthesis of 2-methylbutyrate, isobutyrate and isovalerate, the short/branched-chain fatty acids regulated by BCKDK (Cole, 2015) during effector memory formation in T/NIX$^{-/-}$ Ova-CD8$^+$ T cells, as measured by liquid chromatography-mass spectrometry (LC-MS) (Figures S6A and S6B). These data suggest a shift from long-chain fatty acid oxidation to short/branched fatty acid oxidation during effector memory formation in T/NIX$^{-/-}$ Ova-specific CD8$^+$ T cells.

We next induced effector memory formation in Ova-specific CD8$^+$ T cells *in vitro* in the presence of CAY10585, an inhibitor of HIF1α accumulation (Lee et al., 2007), and observed complete restoration of *Fasn* (Figure 6D) and *Bckdk* (Figure 6D) expression in T/NIX$^{-/-}$ CD8$^+$ T cells. Likewise, treatment with NAC during the contraction phase also restored expression of both *Fasn* (Figure S6C) and *Bckdk* (Figure S6D) during effector memory formation in T/NIX$^{-/-}$ mice. We next measured mitochondrial respiration in Ova-EM by extracellular flux analysis, which quantifies oxygen consumption rate (OCR) in real time. Decreased OCR after addition of etomoxir, an inhibitor of long-chain fatty

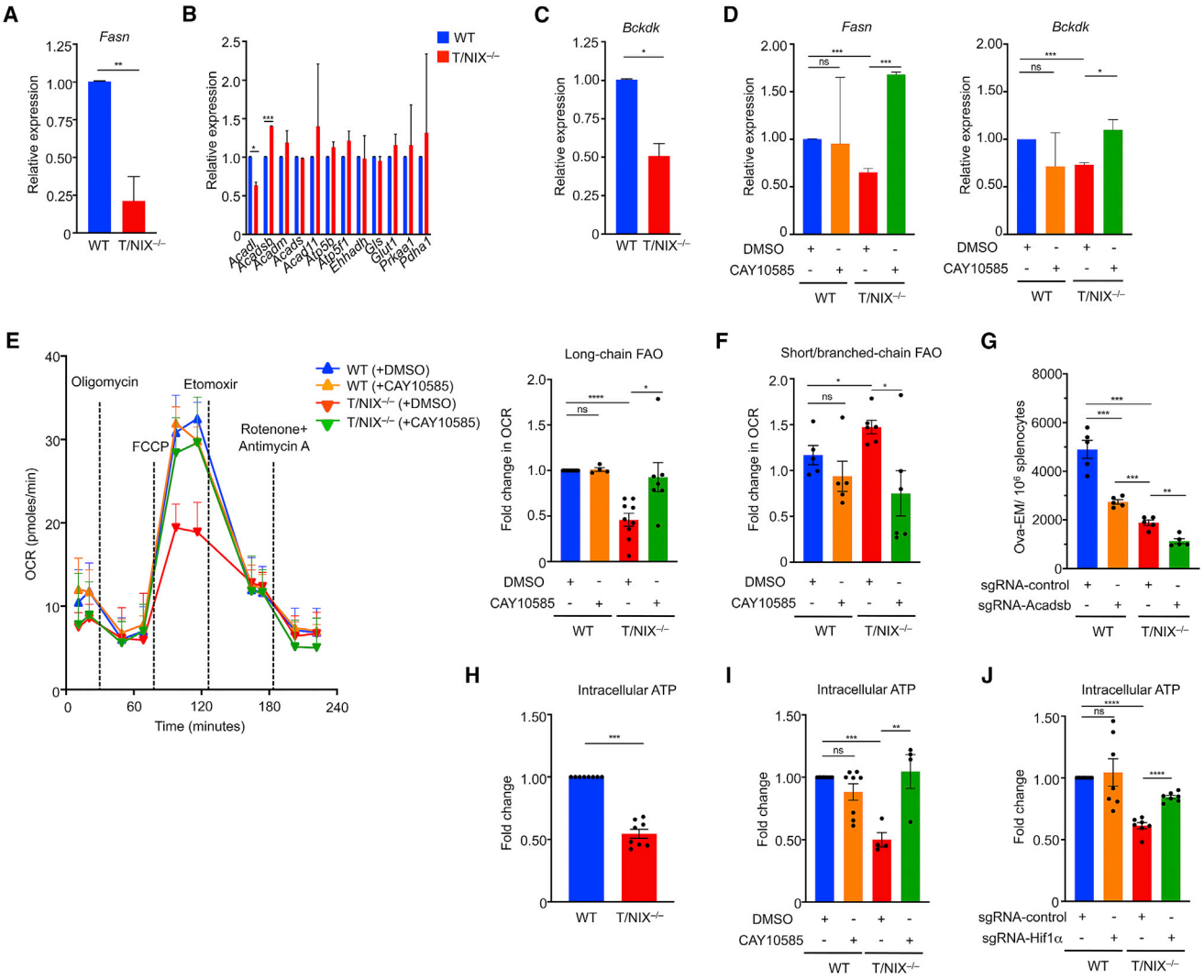

Figure 6. Elevated HIF1α Alters Mitochondrial Fatty Acid Metabolism during CD8$^+$ T Cell Effector Memory Formation in T/NIX$^{-/-}$ Mice, Leading to Impairment in ATP Synthesis

(A) Gene expression of *Fasn* in Ova-EM 30 days after immunization with 10^4 VSV-Ova.

(B and C) Gene expression of T cell metabolic genes (B) and *Bckdk* (C) in Ova-EM 30 days after VSV-Ova immunization in WT and T/NIX$^{-/-}$ mice.

(D) Gene expression of *Fasn* (left panel) and *Bckdk* (right panel) in Ova-EM formed *in vitro* (vehicle or CAY10585 treatment on day 4).

(E) Left: representative OCR in Ova-EM *in vitro* (vehicle or CAY10585 treated OT-I WT and OT-I T/NIX$^{-/-}$ cells). Right: fold change in long-chain fatty acid oxidation-linked OCR from left panel.

(F) Fold change in short/branched-chain fatty acid oxidation linked OCR in Ova-EM formed *in vitro* (vehicle or CAY10585 treated OT-I WT and OT-I T/NIX$^{-/-}$ cells).

(G) Effect of loss of ACADSB on effector memory formation in OT-I WT and OT-I T/NIX$^{-/-}$ cells transduced with LentiCRISPRv2 expressing sgRNA-control or sgRNA-ACADSB.

(H) Intracellular ATP level in Ova-EM 30 days p.i. in WT and T/NIX$^{-/-}$ mice.

(I) Intracellular ATP in Ova-EM formed *in vitro* (vehicle or CAY10585 treated WT or T/NIX$^{-/-}$ cells).

(J) Intracellular ATP in Ova-EM formed *in vitro* (sgRNA-control or sgRNA-HIF1α transduced OT-I WT or OT-I T/NIX$^{-/-}$ cells).

Ova-EM from all mice within the same experimental group in (A)–(F) and (H)–(J) were pooled for analysis. Each point represents an individual independent experiment. Data are representative of two or more independent experiments (n = 4–9). Data were analyzed using two-tailed Student's t test (mean ± SEM). *$p < 0.05$, **$p < 0.01$, and ***$p < 0.001$. ns, non-significant. See also Figures S6 and S7.

acid oxidation (Pike et al., 2011), represented the extent to which Ova-EM carried out long-chain fatty acid oxidation. Long-chain fatty acid metabolism was significantly impaired in T/NIX$^{-/-}$ Ova-EM but was restored upon HIF1α inhibition by CAY10585 during effector memory formation (Figure 6E). We also verified upregulation of short/branched-chain fatty acid metabolism during effector memory formation in T/NIX$^{-/-}$ CD8$^+$ T cells via extracellular flux analysis. We measured any change in OCR upon addition of BCAAs to Ova-EM that were cultured in BCAA-free media during the measurement. Consistent with

reduced BCKDK (Figure 6C) and increased ACADSB (Figure 6B), OCR in T/NIX$^{-/-}$ Ova-EM increased upon addition of BCAAs, which was reversed after treatment with CAY10585 (Figure 6F). Additionally, we found that short/branched-chain fatty acid oxidation played a critical role in partially rescuing the formation of effector memory in T/NIX$^{-/-}$ CD8$^+$ T cells because knocking out ACADSB (Figures S7A and S7B) reduced effector memory formation even further (Figure 6G). Interestingly, short/branched-chain fatty acid oxidation was found to be critical for effector memory formation in WT CD8$^+$ T cells as well (Figure 6G), suggesting that short/branched-chain fatty acid oxidation might be a critical metabolic pathway in addition to long-chain fatty acid oxidation during CD8$^+$ T cell effector memory formation. These data indicate that elevated HIF1α "sHIFted" the metabolism from long-chain fatty acid oxidation to short/branched-chain fatty acid oxidation during CD8$^+$ T cell effector memory formation in T/NIX$^{-/-}$ mice. Additionally, treatment of ACADSB$^{-/-}$ CD8$^+$ T cells with rapamycin modestly improved effector memory formation only in WT, but not T/NIX$^{-/-}$ CD8$^+$ T cells, and was unable to achieve a complete restoration (Figure S7C).

Because the length of metabolized fatty acids dictates the amount of ATP generated (Carracedo et al., 2013), increased dependence on short/branched fatty acid metabolism in T/NIX$^{-/-}$ mice could potentially compromise ATP generation during CD8$^+$ T cell effector memory formation. We observed a significant reduction in ATP synthesis in T/NIX$^{-/-}$ Ova-EM compared with WT Ova-EM (Figure 6H) that was restored upon removing mitochondrial superoxide during contraction phase in T/NIX$^{-/-}$ mice (Figure S7D). Furthermore, ATP synthesis was restored in T/NIX$^{-/-}$ Ova-specific CD8$^+$ T cells during effector memory formation in the presence of CAY10585 (Figure 6I). We also used LentiCRISPRv2-mediated CRISPR-Cas9 genome editing (sgRNA-HIF1α) to knockout HIF1α (Figures S7E and S7F) in CD8$^+$ T cells during effector memory formation. Because deleting HIF1α early during the activation of CD8$^+$ T cells prevented their survival (Figure S7G), we performed LentiCRISPRv2-mediated HIF1α deletion on day 3 post-activation in CD8$^+$ T cells and achieved a selective transduction in post-activated CD8$^+$ T cells (91.65% $\pm$ 2.17% for sgRNA-HIF1α and 72.45% $\pm$ 1.318% for sgRNA-HIF1α^{2nd}) (Figures S7H and S7I). Upon ablation of HIF1α from post-activated T/NIX$^{-/-}$ Ova-CD8$^+$, ATP synthesis was restored during effector memory formation (Figure 6J). These data suggest that elevated HIF1α during effector memory formation in T/NIX$^{-/-}$ antigen-specific CD8$^+$ T cells switched metabolism from long-chain fatty acid oxidation to short/branched-chain fatty acid oxidation, resulting in decreased ATP synthesis.

Inhibiting HIF1α Accumulation Restores Effector Memory Formation in Antigen-Specific T/NIX$^{-/-}$ CD8$^+$ T Cells

Finally, we explored if restoring mitochondrial fatty acid metabolism and ATP synthesis by inhibiting HIF1α would also restore effector memory formation in T/NIX$^{-/-}$ CD8$^+$ T cells. We found that impaired effector memory formation in these cells was rescued upon treatment with CAY10585 (Figures 7A and 7B) and CRISPR-Cas9-mediated deletion of HIF1α (Figures 7C and S7J).

We next investigated whether the impairment in effector memory formation in T/NIX$^{-/-}$CD8$^+$ T cells was a result of defective ATP synthesis. We induced CD8$^+$ T cell effector memory formation *in vitro* in the presence of both CAY10585 and oligomycin, an inhibitor of mitochondrial ATP synthesis. Treatment with oligomycin abolished the restoration of effector memory formation in T/NIX$^{-/-}$CD8$^+$ T cells that was otherwise achieved by CAY10585 treatment (Figure 7D), suggesting that the defective effector memory formation due to HIF1α accumulation in T/NIX$^{-/-}$CD8$^+$ T cells was ultimately caused by insufficient ATP generation. In addition, treatment with oligomycin impaired effector memory formation in WT CD8$^+$ T cells to a level comparable with that in vehicle-treated T/NIX$^{-/-}$CD8$^+$ T cells (Figure 7D), further supporting that inadequate mitochondrial ATP synthesis was the cause of impaired effector memory formation in T/NIX$^{-/-}$CD8$^+$ T cells. These data suggest that HIF1α-mediated suppression of ATP generation was responsible for the impaired effector memory formation in antigen-specific T/NIX$^{-/-}$ CD8$^+$ T cells.

We further observed that in VSV-Ova-infected mice that were pre-injected with WT or T/NIX$^{-/-}$ Ova-EM, T/NIX$^{-/-}$ Ova-EM-recipient mice had significantly reduced concentration of IFN-γ after infection (Figure 7E). In contrast, CAY10585-treated T/NIX$^{-/-}$ Ova-EM-recipient mice had restored IFN-γ production (Figure 7E). IFN-γ plays a pivotal role in the protective immunity against intracellular viral infections (Lauvau and Soudja, 2015). Consistently, mice that received vehicle-treated T/NIX$^{-/-}$ Ova-EM had higher viral load, and this defect was rescued in mice that received CAY10585-treated T/NIX$^{-/-}$ Ova-EM (Figure 7F). These data highlight a pivotal role of HIF1α in impairing effector memory formation in T/NIX$^{-/-}$ antigen-specific CD8$^+$ T cells, leading to a compromised immunity against cytopathic viral infection.

DISCUSSION

We show that deficiency in NIX-dependent mitophagy leads to increased apoptosis in CD8$^+$ MPECs and defective differentiation of effector memory CD8$^+$ T cells. Moreover, impaired mitophagy resulted in the accumulation of mitochondrial superoxide and HIF1α in virus-specific CD8$^+$ T cells during contraction phase. This promoted short/branched-chain fatty acid oxidation at the expense of long-chain fatty acid oxidation, thereby decreasing ATP synthesis, negatively affecting CD8$^+$ T cell effector memory formation and compromising recall response against cytopathic viral infection.

Our study also demonstrates that TCR signaling during primary response downregulates NIX expression in virus-specific activated CD8$^+$ T cells. Downregulation of NIX could allow accumulation of depolarized mitochondria, which is required to mediate optimal T cell activation (Baixauli et al., 2011) via mitochondrial superoxide (Desdin-Mico et al., 2018). However, upon entering contraction phase, these antigen-specific CD8$^+$ T cells upregulate their NIX expression to clear off superoxide-generating depolarized mitochondria to form optimal effector memory against the virus. We further found that IL-15 signaling upregulated *Nix* expression *in vitro*. However, whether IL-15 signaling is required to upregulate NIX expression *in vivo* remains to be determined.

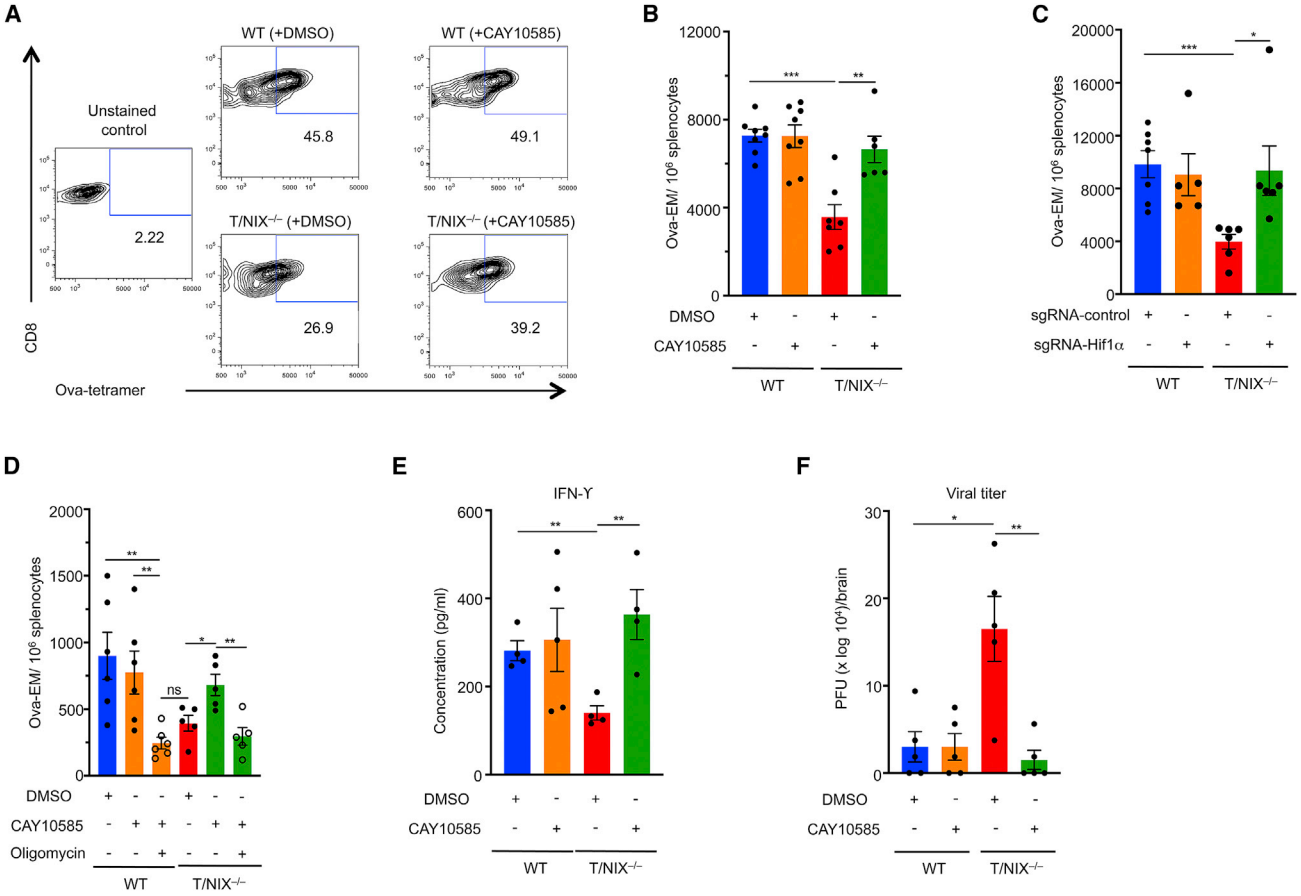

Figure 7. Inhibiting HIF1α Accumulation Restores Effector Memory Formation in Antigen-Specific T/NIX$^{-/-}$ CD8^{+} T cells

(A) Representative plot showing percentage of Ova-EM formed *in vitro* from WT and T/NIX$^{-/-}$ splenocytes (treated with vehicle or CAY10585 on day 4).

(B) Mean frequency of Ova-EM from (A).

(C) Effect of loss of HIF1α on effector memory formation. OT-I WT or OT-I T/NIX$^{-/-}$ cells were transduced with LentiCRISPRv2 expressing sgRNA-HIF1α or sgRNA-control. Ova-EM from all mice within the same experimental group were combined. Each point represents an individual independent experiment.

(D) Mean frequency of Ova-EM formed *in vitro* from WT and T/NIX$^{-/-}$ splenocytes (treated with CAY10585 or CAY10585 and oligomycin).

(E and F) IFN-ϒ concentration in the spleen (E) and (F) viral titer in the brains of mice 48 h after infection with 10^6 PFU of VSV-Ova. Naive C57/BL6J mice were injected with vehicle or CAY10585-treated WT or T/NIX$^{-/-}$ cells, generated as in (A), followed by infection with VSV-Ova.

Data in (A)–(D) are representative of two or more independent experiments (n = 5–8), and data in (E) and (F) are representative of four or five biological replicates per group. Data were analyzed by two-tailed Student's t test (mean ± SEM). *$p < 0.05$, **$p < 0.01$, and ***$p < 0.001$. ns, non-significant. See also Figure S7.

Loss of NIX led to mitochondrial accumulation in effector memory, but not naive or central memory, CD8^{+} T cells, suggesting that NIX-mediated mitophagy plays a selective role in CD8^{+} T cell effector memory formation. It is intriguing how NIX plays a tissue-specific role during T cell effector memory formation but not central memory formation. It could be related to chromatin remodeling unique to effector memory development. In fact, chromatin remodeling unique to the development of tissue-resident memory T cells has been reported to predispose RUNX3 to selectively favor differentiation of tissue-resident memory T cells over central or effector memory T cells (Milner et al., 2017). These unique chromatin landscapes favoring the formation of different subsets of memory T cells could in turn be regulated by unique DNA methylation patterns determining the fate of memory in virus-specific T cells (Akondy et al., 2017; Youngblood et al., 2017). Alternatively, other molecules might play a more pivotal role in mediating mitophagy in central memory population. FUNDC1 and BCL2L13, which are also outer mitochondrial membrane proteins, have also been reported to mediate mitophagy in mammalian cells (Liu et al., 2012; Murakawa et al., 2015; Rodger et al., 2018). Hence, it is possible that these molecules might regulate mitophagy during T cell central memory formation. These possibilities, however, need to be experimentally verified through future studies.

Impaired mitophagy during effector memory formation in T/NIX$^{-/-}$ CD8^{+} T cells further led to excessive mitochondrial superoxide during contraction phase. Although mitochondrial superoxide is necessary for CD8^{+} T cell primary response (Kaminski et al., 2010; Murphy and Siegel, 2013), our data suggest that its continued presence during contraction phase blocks effector memory formation. Mitochondrial superoxide caused HIF1α accumulation during the contraction phase of effector

memory formation in T/NIX$^{-/-}$ mice. Scavenging mitochondrial superoxide significantly reduced HIF1α protein accumulation. We also found that blocking HIF1α expression early during T cell activation reduced frequency of activated CD8$^+$ T cells, suggesting that HIF1α is necessary for activation of these cells, likely because of its role in upregulating glycolysis (Lee and Simon, 2012; Pollizzi and Powell, 2014; Menk et al., 2018; van der Windt et al., 2012). However, continued presence of HIF1α during contraction phase was detrimental to CD8$^+$ T cell effector memory formation in T/NIX$^{-/-}$ mice.

We also found that accumulation of HIF1α during effector-to-memory transition in T/NIX$^{-/-}$ CD8$^+$ T cells "sHIFted" their metabolism to short/branched-chain fatty acid oxidation, which was unexpected because this pathway is less efficient in generating ATP compared with alternative pathways, especially very long chain fatty acid oxidation, which did not alter in the absence of NIX. One explanation for choosing short/branched-chain fatty acids over very long chain fatty acids by T/NIX$^{-/-}$ CD8$^+$ T cells might be that the former can readily diffuse into the mitochondrial matrix (den Besten et al., 2013) as opposed to very long chain fatty acids, which require ATP-dependent active transporters (Jia et al., 2007; Watkins et al., 1998). Hence, catabolizing short/branched-chain fatty acids was probably bioenergetically more favorable during effector memory formation in T/NIX$^{-/-}$ CD8$^+$ T cells, which were already deficient in ATP during contraction phase. Short-chain fatty acids did not play a significant role during effector memory formation either, possibly because of mammalian cells' inability to synthesize short-chain fatty acids *de novo*, which they obtain from gut bacteria (den Besten et al., 2013); thus, absence of NIX in CD8$^+$ T cells would not likely alter the supply of short-chain fatty acids. Medium-chain fatty acids would be expected to be less efficient than short/branched-chain fatty acids in diffusing into mitochondria, because of sterically bulkier carbon chain. All these reasons probably left short/branched-chain fatty acid oxidation as the best alternative during effector memory formation in T/NIX$^{-/-}$ CD8$^+$ T cells. It is also interesting that short/branched-chain fatty acid oxidation played a critical role at an early stage during CD8$^+$ T cell effector memory formation, and deletion of NIX likely promoted this pathway to compensate for the impaired long-chain fatty acid metabolism during effector memory formation. Because enhancing long-chain fatty acid oxidation has been shown to improve T cell memory formation (van der Windt et al., 2012), it is possible that overexpression of FASN in ACADSB$^{-/-}$ CD8$^+$ T cells could improve effector memory formation as well. However, this needs to be further tested.

NK cells are dependent on BNIP3 but only partially reliant on NIX for their survival through the contraction phase (O'Sullivan et al., 2015). Interestingly, we found that NIX is required for optimal generation of CD8$^+$ effector memory, whereas BNIP3 is dispensable. This suggests that NIX and BNIP3, two homologous proteins, may play tissue-specific roles in different cell types. We further found that PINK1 and PARK2, another set of mitophagy molecules, were not significantly upregulated during memory formation. Consistently, reduced frequency of CD8$^+$ T cells was not detected on day 13 p.i. in PINK1$^{-/-}$ mice either (Matheoud et al., 2019). In addition, deletion of *Pink1* did not alter mitochondrial stress and long-chain fatty acid metabolism in T cells (Ellis et al., 2013). Together, these data suggest a non-critical role of PINK1 during CD8$^+$ T cell memory formation. PARK2, which is activated by PINK1 (Gladkova et al., 2018), was temporally downregulated during memory formation, consistent with no reduction in T cell frequency in absence of PARK2 during viral infection, as reported elsewhere (Li et al., 2019). Although the exact mechanism of *Park2* downregulation during T cell memory formation needs to be further elucidated, one possible mechanism could be related to midnolin (*Midn*) expression, which mediates gene expression of *Park2* (Obara and Ishii, 2018) and has also been reported to be expressed in T cells (Hashimoto et al., 2013). However, whether *Park2* downregulation during T cell memory formation is regulated by midnolin is a subject for future studies. Taken together, these data suggest that despite their roles in regulating mitophagy, PINK1 and PARK2 likely do not play a critical role as NIX does in T cell memory formation.

To date, the development of successful vaccines against several viral pathogens has been challenged by the inability of vaccines to elicit a robust CD8$^+$ T cell effector memory formation (van Duikeren et al., 2012; Sallusto et al., 2010). Efficacy of experimental cancer vaccines has also been found to depend on the strength of immunological memory formation in tumor-specific T cells (Beckhove et al., 2004; Hu and Wang, 2017). In addition, T cell effector memory formation against auto-antigens has been shown to exacerbate the symptoms associated with auto-immune disorders, and inhibition of auto-antigen-specific effector memory T cells could alleviate those symptoms (Bhargava and Calabresi, 2015; Beeton et al., 2005; Beeton et al., 2006; Chee et al., 2014; Matheu et al., 2008). Our findings have implications for advancing the fields of vaccine, cancer immunotherapy, and auto-immunity research by targeting NIX, HIF1α, and metabolism of long-chain as well as short/branched-chain fatty acids.

STAR★METHODS

Detailed methods are provided in the online version of this paper and include the following:

- KEY RESOURCES TABLE
- LEAD CONTACT AND MATERIALS AVAILABILITY
- EXPERIMENTAL MODEL AND SUBJECT DETAILS
  - Animals
  - Cell lines and primary cell cultures
- METHOD DETAILS
  - Virus, immunization and infection
  - Flow cytometry
  - CD8$^+$ population enrichment and cell sorting
  - Effector memory formation in CD8$^+$ T cells *in vitro*
  - Adoptive transfer
  - Quantitative PCR and PCR array of metabolic genes
  - Measurement of apoptosis in Ova-CD8$^+$ MPECs and Ova-EM
  - Immunocytochemistry
  - Measurement of mitochondrial membrane depolarization
  - Mitochondrial DNA damage assay
  - Drug treatments

- Intracellular staining
- CRISPR/Cas9-mediated deletion of Hif1α and Acadsb genes
- Western blotting
- Viral titer assays
- Serum isolation and ELISA
- Measurement of short/branched-chain fatty acids
- Extracellular flux analysis (Seahorse assay)
- ATP assay

- QUANTIFICATION AND STATISTICAL ANALYSIS
- DATA AND CODE AVAILABILITY

SUPPLEMENTAL INFORMATION

Supplemental Information can be found online at https://doi.org/10.1016/j.celrep.2019.10.032.

ACKNOWLEDGMENTS

We thank Jay Dunn for advice on extracellular flux analysis; Albert Jang for technical assistance; Farah Kheradmand, David Corry, Tony Eissa, George Makedonas, Matthew Bettini, and Hana El Sahly for discussions; and Nagireddy Putluri for analyses of short/branched-chain fatty acids. This work was supported by grants from the American Heart Association to M.C (15GRNT25700357), the Cancer Prevention Research Institute of Texas (CPRIT) to M.C. and J.W. (RP160384), the NIH to J.W. (R01 AI116644 and R01 AI123221) and to G.W.D. (R35HL135736), and the Lupus Research Institute to M.C. and J.W. We acknowledge technical support from Baylor College of Medicine's Cytometry and Cell Sorting Core, with funding from the NIH (P30 AI036211, P30 CA125123, and S10 RR024574); Integrated Microscopy Core, with funding from the NIH (DK56338 and CA125123) and the CPRIT (RP150578), the Dan L. Duncan Comprehensive Cancer Center (DLDCC), and the John S. Dunn Gulf Coast Consortium for Chemical Genomics; Mouse Metabolism and Phenotyping Core, with funding from the NIH (RO1DK114356 and UM1HG006348) and CPRIT Core Facility Support Award (RP170005), "Proteomic and Metabolomic Core Facility" with NCI Cancer Center Support Grant (P30CA125123), and DLDCC intramural funds.

AUTHOR CONTRIBUTIONS

S.S.G., R.S., and C.H. performed experiments involving flow cytometry. L.K. performed the thymic T cell development study. S.S.G. analyzed data and performed the rest of the experiments. G.D. generated $NIX^{f/f}$ mice. S.S.G. planned studies, designed experiments, and wrote the manuscript. M.C. and J.W. supervised the study and edited the manuscript.

DECLARATION OF INTERESTS

The authors declare no competing interests.

Received: June 11, 2019
Revised: September 4, 2019
Accepted: October 9, 2019
Published: November 12, 2019

REFERENCES

Akondy, R.S., Fitch, M., Edupuganti, S., Yang, S., Kissick, H.T., Li, K.W., Youngblood, B.A., Abdelsamed, H.A., McGuire, D.J., Cohen, K.W., et al. (2017). Origin and differentiation of human memory CD8 T cells after vaccination. Nature *552*, 362–367.

Alfardan, J., Mohsen, A.-W., Copeland, S., Ellison, J., Keppen-Davis, L., Rohrbach, M., Powell, B.R., Gillis, J., Matern, D., Kant, J., and Vockley, J. (2010). Characterization of new *ACADSB* gene sequence mutations and clinical implications in patients with 2-methylbutyrylglycinuria identified by newborn screening. Mol. Genet. Metab. *100*, 333–338.

Almeida, L., Lochner, M., Berod, L., and Sparwasser, T. (2016). Metabolic pathways in T cell activation and lineage differentiation. Semin. Immunol. *28*, 514–524.

Araujo, L.F., Siena, A.D.D., Plaça, J.R., Brotto, D.B., Barros, I.I., Muys, B.R., Biagi, C.A.O., Jr., Peronni, K.C., Sousa, J.F., Molfetta, G.A., et al. (2018). Mitochondrial transcription factor A (TFAM) shapes metabolic and invasion gene signatures in melanoma. Sci. Rep. *8*, 14190.

Avery, L., Filderman, J., Szymczak-Workman, A.L., and Kane, L.P. (2018). Tim-3 co-stimulation promotes short-lived effector T cells, restricts memory precursors, and is dispensable for T cell exhaustion. Proc. Natl. Acad. Sci. U S A *115*, 2455–2460.

Baixauli, F., Martín-Cófreces, N.B., Morlino, G., Carrasco, Y.R., Calabia-Linares, C., Veiga, E., Serrador, J.M., and Sánchez-Madrid, F. (2011). The mitochondrial fission factor dynamin-related protein 1 modulates T-cell receptor signalling at the immune synapse. EMBO J. *30*, 1238–1250.

Beckermann, K.E., Dudzinski, S.O., and Rathmell, J.C. (2017). Dysfunctional T cell metabolism in the tumor microenvironment. Cytokine Growth Factor Rev. *35*, 7–14.

Beckhove, P., Feuerer, M., Dolenc, M., Schuetz, F., Choi, C., Sommerfeldt, N., Schwendemann, J., Ehlert, K., Altevogt, P., Bastert, G., et al. (2004). Specifically activated memory T cell subsets from cancer patients recognize and reject xenotransplanted autologous tumors. J. Clin. Invest. *114*, 67–76.

Beeton, C., Pennington, M.W., Wulff, H., Singh, S., Nugent, D., Crossley, G., Khaytin, I., Calabresi, P.A., Chen, C.Y., Gutman, G.A., and Chandy, K.G. (2005). Targeting effector memory T cells with a selective peptide inhibitor of Kv1.3 channels for therapy of autoimmune diseases. Mol. Pharmacol. *67*, 1369–1381.

Beeton, C., Wulff, H., Standifer, N.E., Azam, P., Mullen, K.M., Pennington, M.W., Kolski-Andreaco, A., Wei, E., Grino, A., Counts, D.R., et al. (2006). Kv1.3 channels are a therapeutic target for T cell-mediated autoimmune diseases. Proc. Natl. Acad. Sci. U S A *103*, 17414–17419.

Bengsch, B., Spangenberg, H.C., Kersting, N., Neumann-Haefelin, C., Panther, E., von Weizsäcker, F., Blum, H.E., Pircher, H., and Thimme, R. (2007). Analysis of CD127 and KLRG1 expression on hepatitis C virus-specific CD8+ T cells reveals the existence of different memory T-cell subsets in the peripheral blood and liver. J. Virol. *81*, 945–953.

Bhargava, P., and Calabresi, P.A. (2015). Novel therapies for memory cells in autoimmune diseases. Clin. Exp. Immunol. *180*, 353–360.

Bian, M., Liu, J., Hong, X., Yu, M., Huang, Y., Sheng, Z., Fei, J., and Huang, F. (2012). Overexpression of parkin ameliorates dopaminergic neurodegeneration induced by 1- methyl-4-phenyl-1,2,3,6-tetrahydropyridine in mice. PLoS ONE *7*, e39953.

Billingsley, J.M., Rajakumar, P.A., Connole, M.A., Salisch, N.C., Adnan, S., Kuzmichev, Y.V., Hong, H.S., Reeves, R.K., Kang, H.-J., Li, W., et al. (2015). Characterization of CD8+ T cell differentiation following SIVΔnef vaccination by transcription factor expression profiling. PLoS Pathog. *11*, e1004740.

Bordi, M., Nazio, F., and Campello, S. (2017). The close interconnection between mitochondrial dynamics and mitophagy in cancer. Front. Oncol. *7*, 81.

Buck, M.D.D., O'Sullivan, D., Klein Geltink, R.I., Curtis, J.D., Chang, C.H., Sanin, D.E., Qiu, J., Kretz, O., Braas, D., van der Windt, G.J., et al. (2016). Mitochondrial dynamics controls T cell fate through metabolic programming. Cell *166*, 63–76.

Carracedo, A., Cantley, L.C., and Pandolfi, P.P. (2013). Cancer metabolism: fatty acid oxidation in the limelight. Nat. Rev. Cancer *13*, 227–232.

Chandel, N.S., Maltepe, E., Goldwasser, E., Mathieu, C.E., Simon, M.C., and Schumacker, P.T. (1998). Mitochondrial reactive oxygen species trigger hypoxia-induced transcription. Proc. Natl. Acad. Sci. U S A *95*, 11715–11720.

Chandel, N.S., McClintock, D.S., Feliciano, C.E., Wood, T.M., Melendez, J.A., Rodriguez, A.M., and Schumacker, P.T. (2000). Reactive oxygen species generated at mitochondrial complex III stabilize hypoxia-inducible factor-1α during hypoxia: a mechanism of O2 sensing. J. Biol. Chem. *275*, 25130–25138.

Chee, J., Ko, H.J., Skowera, A., Jhala, G., Catterall, T., Graham, K.L., Sutherland, R.M., Thomas, H.E., Lew, A.M., Peakman, M., et al. (2014). Effector-memory T cells develop in islets and report islet pathology in type 1 diabetes. J. Immunol. *192*, 572–580.

Chen, M., Wang, Y.H., Wang, Y., Huang, L., Sandoval, H., Liu, Y.J., and Wang, J. (2006). Dendritic cell apoptosis in the maintenance of immune tolerance. Science *311*, 1160–1164.

Chen, M., Hong, M.J., Sun, H., Wang, L., Shi, X., Gilbert, B.E., Corry, D.B., Kheradmand, F., and Wang, J. (2014). Essential role for autophagy in the maintenance of immunological memory against influenza infection. Nat. Med. *20*, 503–510.

Chen, M., Kodali, S., Jang, A., Kuai, L., and Wang, J. (2015). Requirement for autophagy in the long-term persistence but not initial formation of memory B cells. J. Immunol. *194*, 2607–2615.

Chirichigno, J.W., Manfredi, G., Beal, M.F., and Albers, D.S. (2002). Stress-induced mitochondrial depolarization and oxidative damage in PSP cybrids. Brain Res. *951*, 31–35.

Cole, J.T. (2015). Metabolism of BCAAs. In Branched Chain Amino Acids in Clinical Nutrition, R. Rajendram, V.R. Preedy, and V. Patel, eds. (Humana Press), pp. 13–24.

D'Souza, W.N., and Hedrick, S.M. (2006). Cutting edge: latecomer CD8 T cells are imprinted with a unique differentiation program. J. Immunol. *177*, 777–781.

Danilo, M., Chennupati, V., Silva, J.G., Siegert, S., and Held, W. (2018). Suppression of Tcf1 by Inflammatory Cytokines Facilitates Effector CD8 T Cell Differentiation. Cell Rep. *22*, 2107–2117.

den Besten, G., van Eunen, K., Groen, A.K., Venema, K., Reijngoud, D.J., and Bakker, B.M. (2013). The role of short-chain fatty acids in the interplay between diet, gut microbiota, and host energy metabolism. J. Lipid Res. *54*, 2325–2340.

Desdin-Mico, G., Soto-Heredero, G., and Mittelbrunn, M. (2018). Mitochondrial activity in T cells. Mitochondrion *41*, 51–57.

Diwan, A., Koesters, A.G., Odley, A.M., Pushkaran, S., Baines, C.P., Spike, B.T., Daria, D., Jegga, A.G., Geiger, H., Aronow, B.J., et al. (2007). Unrestrained erythroblast development in Nix-/- mice reveals a mechanism for apoptotic modulation of erythropoiesis. Proc. Natl. Acad. Sci. U S A *104*, 6794–6799.

Ellis, G.I., Zhi, L., Akundi, R., Büeler, H., and Marti, F. (2013). Mitochondrial and cytosolic roles of PINK1 shape induced regulatory T-cell development and function. Eur. J. Immunol. *43*, 3355–3360.

Ganeshan, K., and Chawla, A. (2014). Metabolic regulation of immune responses. Annu. Rev. Immunol. *32*, 609–634.

Garrod, K.R., Moreau, H.D., Garcia, Z., Lemaître, F., Bouvier, I., Albert, M.L., and Bousso, P. (2012). Dissecting T cell contraction in vivo using a genetically encoded reporter of apoptosis. Cell Rep. *2*, 1438–1447.

Gkikas, I., Palikaras, K., and Tavernarakis, N. (2018). The role of mitophagy in innate immunity. Front. Immunol. *9*, 1283.

Gladkova, C., Maslen, S.L., Skehel, J.M., and Komander, D. (2018). Mechanism of parkin activation by PINK1. Nature *559*, 410–414.

Harrington, L.E., Galvan, M., Baum, L.G., Altman, J.D., and Ahmed, R. (2000). Differentiating between memory and effector CD8 T cells by altered expression of cell surface O-glycans. J. Exp. Med. *191*, 1241–1246.

Harris, R.A., Paxton, R., Powell, S.M., Goodwin, G.W., Kuntz, M.J., and Han, A.C. (1986). Regulation of branched-chain alpha-ketoacid dehydrogenase complex by covalent modification. Adv. Enzyme Regul. *25*, 219–237.

Hashimoto, S., Ogoshi, K., Sasaki, A., Abe, J., Qu, W., Nakatani, Y., Ahsan, B., Oshima, K., Shand, F.H.W., Ametani, A., et al. (2013). Coordinated changes in DNA methylation in antigen-specific memory CD4 T cells. J. Immunol. *190*, 4076–4091.

Herst, P.M., Rowe, M.R., Carson, G.M., and Berridge, M.V. (2017). Functional mitochondria in health and disease. Front. Endocrinol. (Lausanne) *8*, 296.

Hess Michelini, R., Doedens, A.L., Goldrath, A.W., and Hedrick, S.M. (2013). Differentiation of CD8 memory T cells depends on Foxo1. J. Exp. Med. *210*, 1189–1200.

Hikono, H., Kohlmeier, J.E., Takamura, S., Wittmer, S.T., Roberts, A.D., and Woodland, D.L. (2007). Activation phenotype, rather than central- or effector-memory phenotype, predicts the recall efficacy of memory $CD8^+$ T cells. J. Exp. Med. *204*, 1625–1636.

Hu, G., and Wang, S. (2017). Tumor-infiltrating $CD45RO^+$ memory T lymphocytes predict favorable clinical outcome in solid tumors. Sci. Rep. *7*, 10376.

Ježek, J., Cooper, K.F., and Strich, R. (2018). Reactive oxygen species and mitochondrial dynamics: the yin and yang of mitochondrial dysfunction and cancer progression. Antioxidants *7*, 13.

Jia, Z., Moulson, C.L., Pei, Z., Miner, J.H., and Watkins, P.A. (2007). Fatty acid transport protein 4 is the principal very long chain fatty acyl-CoA synthetase in skin fibroblasts. J. Biol. Chem. *282*, 20573–20583.

Jiang, P., Fang, X., Zhao, Z., Yu, X., Sun, B., Yu, H., and Yang, R. (2018). The effect of short/branched chain acyl-coenzyme A dehydrogenase gene on triglyceride synthesis of bovine mammary epithelial cells. Arch. Anim. Breed. *61*, 115–122.

Jin, S.M., and Youle, R.J. (2012). PINK1- and Parkin-mediated mitophagy at a glance. J. Cell Sci. *125*, 795–799.

Jornayvaz, F.R., and Shulman, G.I.G. (2010). Regulation of mitochondrial biogenesis. Essays Biochem. *47*, 69–84.

Joshi, N.S., Cui, W., Chandele, A., Lee, H.K., Urso, D.R., Hagman, J., Gapin, L., and Kaech, S.M. (2007). Inflammation directs memory precursor and short-lived effector CD8(+) T cell fates via the graded expression of T-bet transcription factor. Immunity *27*, 281–295.

Kaech, S.M., and Ahmed, R. (2001). Memory CD8+ T cell differentiation: initial antigen encounter triggers a developmental program in naïve cells. Nat. Immunol. *2*, 415–422.

Kaech, S.M., and Cui, W. (2012). Transcriptional control of effector and memory $CD8^+$ T cell differentiation. Nat. Rev. Immunol. *12*, 749–761.

Kaminski, M.M., Sauer, S.W., Klemke, C.D., Süss, D., Okun, J.G., Krammer, P.H., and Gülow, K. (2010). Mitochondrial reactive oxygen species control T cell activation by regulating IL-2 and IL-4 expression: mechanism of ciprofloxacin-mediated immunosuppression. J. Immunol. *184*, 4827–4841.

Kang, D., and Hamasaki, N. (2003). Mitochondrial oxidative stress and mitochondrial DNA. Clin. Chem. Lab. Med. *41*, 1281–1288.

Kapoor, V.N., Shin, H.M., Cho, O.H., Berg, L.J., Kang, J., and Welsh, R.M. (2014). Regulation of tissue-dependent differences in CD8+ T cell apoptosis during viral infection. J. Virol. *88*, 9490–9503.

Kim, M.V., Ouyang, W., Liao, W., Zhang, M.Q., and Li, M.O. (2013). The transcription factor Foxo1 controls central-memory $CD8^+$ T cell responses to infection. Immunity *39*, 286–297.

Kurtz, D.M., Rinaldo, P., Rhead, W.J., Tian, L., Millington, D.S., Vockley, J., Hamm, D.A., Brix, A.E., Lindsey, J.R., Pinkert, C.A., et al. (1998). Targeted disruption of mouse long-chain acyl-CoA dehydrogenase gene reveals crucial roles for fatty acid oxidation. Proc. Natl. Acad. Sci. U S A *95*, 15592–15597.

Lauvau, G., and Soudja, S.M. (2015). Mechanisms of memory T cell activation and effective immunity. Adv. Exp. Med. Biol. *850*, 73–80.

Lee, K.E., and Simon, M.C. (2012). From stem cells to cancer stem cells: HIF takes the stage. Curr. Opin. Cell Biol. *24*, 232–235.

Lee, K., Lee, J.H., Boovanahalli, S.K., Jin, Y., Lee, M., Jin, X., Kim, J.H., Hong, Y.S., and Lee, J.J. (2007). (Aryloxyacetylamino)benzoic acid analogues: a new class of hypoxia-inducible factor-1 inhibitors. J. Med. Chem. *50*, 1675–1684.

Leong, Y.A., Chen, Y., Ong, H.S., Wu, D., Man, K., Deleage, C., Minnich, M., Meckiff, B.J., Wei, Y., Hou, Z., et al. (2016). CXCR5(+) follicular cytotoxic T cells control viral infection in B cell follicles. Nat. Immunol. *17*, 1187–1196.

Li, J., Ma, C., Long, F., Yang, D., Liu, X., Hu, Y., Wu, C., Wang, B., Wang, M., Chen, Y., et al. (2019). Parkin impairs antiviral immunity by suppressing the mitochondrial reactive oxygen species-Nlrp3 axis and antiviral inflammation. iScience *16*, 468–484.

Lin, W.W., Nish, S.A., Yen, B., Chen, Y.H., Adams, W.C., Kratchmarov, R., Rothman, N.J., Bhandoola, A., Xue, H.H., and Reiner, S.L. (2016). $CD8^+$ T

lymphocyte self-renewal during effector cell determination. Cell Rep. *17*, 1773–1782.

Liu, L., Feng, D., Chen, G., Chen, M., Zheng, Q., Song, P., Ma, Q., Zhu, C., Wang, R., Qi, W., et al. (2012). Mitochondrial outer-membrane protein FUNDC1 mediates hypoxia-induced mitophagy in mammalian cells. Nat. Cell Biol. *14*, 177–185.

Luís, P.B.M., Ruiter, J.P.N., Ijlst, L., Tavares de Almeida, I., Duran, M., Mohsen, A.W., Vockley, J., Wanders, R.J., and Silva, M.F. (2011). Role of isovaleryl-CoA dehydrogenase and short branched-chain acyl-CoA dehydrogenase in the metabolism of valproic acid: implications for the branched-chain amino acid oxidation pathway. Drug Metab. Dispos. *39*, 1155–1160.

Masopust, D., Vezys, V., Marzo, A.L., and Lefrançois, L. (2001). Preferential localization of effector memory cells in nonlymphoid tissue. Science *291*, 2413–2417.

Matheoud, D., Cannon, T., Voisin, A., Penttinen, A.-M., Ramet, L., Fahmy, A.M., Ducrot, C., Laplante, A., Bourque, M.-J., Zhu, L., et al. (2019). Intestinal infection triggers Parkinson's disease-like symptoms in Pink1$^{-/-}$ mice. Nature *571*, 565–569.

Matheu, M.P., Beeton, C., Garcia, A., Chi, V., Rangaraju, S., Safrina, O., Monaghan, K., Uemura, M.I., Li, D., Pal, S., et al. (2008). Imaging of effector memory T cells during a delayed-type hypersensitivity reaction and suppression by Kv1.3 channel block. Immunity *29*, 602–614.

Matsushima, M., Fujiwara, T., Takahashi, E., Minaguchi, T., Eguchi, Y., Tsujimoto, Y., Suzumori, K., and Nakamura, Y. (1998). Isolation, mapping, and functional analysis of a novel human cDNA (*BNIP3L*) encoding a protein homologous to human NIP3. Genes Chromosomes Cancer *21*, 230–235.

McNamee, E.N., Korns Johnson, D., Homann, D., and Clambey, E.T. (2013). Hypoxia and hypoxia-inducible factors as regulators of T cell development, differentiation, and function. Immunol. Res. *55*, 58–70.

Menk, A.V., Scharping, N.E., Moreci, R.S., Zeng, X., Guy, C., Salvatore, S., Bae, H., Xie, J., Young, H.A., Wendell, S.G., and Delgoffe, G.M. (2018). Early TCR signaling induces rapid aerobic glycolysis enabling distinct acute T cell effector functions. Cell Rep. *22*, 1509–1521.

Milner, J.J., Toma, C., Yu, B., Zhang, K., Omilusik, K., Phan, A.T., Wang, D., Getzler, A.J., Nguyen, T., Crotty, S., et al. (2017). Runx3 programs CD8^{+} T cell residency in non-lymphoid tissues and tumours. Nature *552*, 253–257.

Murakawa, T., Yamaguchi, O., Hashimoto, A., Hikoso, S., Takeda, T., Oka, T., Yasui, H., Ueda, H., Akazawa, Y., Nakayama, H., et al. (2015). Bcl-2-like protein 13 is a mammalian Atg32 homologue that mediates mitophagy and mitochondrial fragmentation. Nat. Commun. *6*, 7527.

Murera, D., Arbogast, F., Arnold, J., Bouis, D., Muller, S., and Gros, F. (2018). CD4 T cell autophagy is integral to memory maintenance. Sci. Rep. *8*, 5951.

Murphy, M.P., and Siegel, R.M. (2013). Mitochondrial ROS fire up T cell activation. Immunity *38*, 201–202.

Obara, Y., and Ishii, K. (2018). Transcriptome Analysis Reveals That Midnolin Regulates mRNA Expression Levels of Multiple Parkinson's Disease Causative Genes. Biol. Pharm. Bull. *41*, 20–23.

O'Sullivan, D., van der Windt, G.J., Huang, S.C., Curtis, J.D., Chang, C.H., Buck, M.D., Qiu, J., Smith, A.M., Lam, W.Y., DiPlato, L.M., et al. (2014). Memory CD8(+) T cells use cell-intrinsic lipolysis to support the metabolic programming necessary for development. Immunity *41*, 75–88.

O'Sullivan, T.E., Johnson, L.R., Kang, H.H., and Sun, J.C. (2015). BNIP3- and BNIP3L-mediated mitophagy promotes the generation of natural killer cell memory. Immunity *43*, 331–342.

Olson, J.A., McDonald-Hyman, C., Jameson, S.C., and Hamilton, S.E. (2013). Effector-like CD8^{+} T cells in the memory population mediate potent protective immunity. Immunity *38*, 1250–1260.

Pike, L.S., Smift, A.L., Croteau, N.J., Ferrick, D.A., and Wu, M. (2011). Inhibition of fatty acid oxidation by etomoxir impairs NADPH production and increases reactive oxygen species resulting in ATP depletion and cell death in human glioblastoma cells. Biochim. Biophys. Acta *1807*, 726–734.

Pollizzi, K.N., and Powell, J.D. (2014). Integrating canonical and metabolic signalling programmes in the regulation of T cell responses. Nat. Rev. Immunol. *14*, 435–446.

Porter, B.B., and Harty, J.T. (2006). The onset of CD8^{+}-T-cell contraction is influenced by the peak of *Listeria monocytogenes* infection and antigen display. Infect. Immun. *74*, 1528–1536.

Puleston, D.J., Zhang, H., Powell, T.J., Lipina, E., Sims, S., Panse, I., Watson, A.S., Cerundolo, V., Townsend, A.R., Klenerman, P., and Simon, A.K. (2014). Autophagy is a critical regulator of memory CD8($^{+}$) T cell formation. eLife *3*, 1–21.

Putluri, N., Shojaie, A., Vasu, V.T., Nalluri, S., Vareed, S.K., Putluri, V., Vivekanandan-Giri, A., Byun, J., Pennathur, S., Sana, T.R., et al. (2011a). Metabolomic profiling reveals a role for androgen in activating amino acid metabolism and methylation in prostate cancer cells. PLoS ONE *6*, e21417.

Putluri, N., Maity, S., Kommagani, R., Creighton, C.J., Putluri, V., Chen, F., Nanda, S., Bhowmik, S.K., Terunuma, A., Dorsey, T., et al. (2014). Pathway-centric integrative analysis identifies RRM2 as a prognostic marker in breast cancer associated with poor survival and tamoxifen resistance. Neoplasia *16*, 390–402.

Qu, A., Taylor, M., Xue, X., Matsubara, T., Metzger, D., Chambon, P., Gonzalez, F.J., and Shah, Y.M. (2011). Hypoxia-inducible transcription factor 2α promotes steatohepatitis through augmenting lipid accumulation, inflammation, and fibrosis. Hepatology *54*, 472–483.

Robbins, S.H., Terrizzi, S.C., Sydora, B.C., Mikayama, T., and Brossay, L. (2003). Differential regulation of killer cell lectin-like receptor G1 expression on T cells. J. Immunol. *170*, 5876–5885.

Rodger, C.E., McWilliams, T.G., and Ganley, I.G. (2018). Mammalian mitophagy - from *in vitro* molecules to *in vivo* models. FEBS J. *285*, 1185–1202.

Rutishauser, R.L., Martins, G.A., Kalachikov, S., Chandele, A., Parish, I.A., Meffre, E., Jacob, J., Calame, K., and Kaech, S.M. (2009). Blimp-1 promotes terminal differentiation of virus-specific CD8 T cells and represses the acquisition of central memory T cell properties. Immunity *31*, 296–308.

Sabbagh, L., Kaech, S.M., Bourbonnière, M., Woo, M., Cohen, L.Y., Haddad, E.K., Labrecque, N., Ahmed, R., and Sékaly, R.P. (2004). The selective increase in caspase-3 expression in effector but not memory T cells allows susceptibility to apoptosis. J. Immunol. *173*, 5425–5433.

Sabins, N.C., Chornoguz, O., Leander, K., Kaplan, F., Carter, R., Kinder, M., Bachman, K., Verona, R., Shen, S., Bhargava, V., and Santulli-Marotto, S. (2017). TIM-3 engagement promotes effector memory T cell differentiation of human antigen-specific CD8 T cells by activating mTORC1. J. Immunol. *199*, 4091–4102.

Sallusto, F., Lenig, D., Förster, R., Lipp, M., and Lanzavecchia, A. (1999). Two subsets of memory T lymphocytes with distinct homing potentials and effector functions. Nature *401*, 708–712.

Sallusto, F., Lanzavecchia, A., Araki, K., and Ahmed, R. (2010). From vaccines to memory and back. Immunity *33*, 451–463.

Sandoval, H., Thiagarajan, P., Dasgupta, S.K., Schumacher, A., Prchal, J.T., Chen, M., and Wang, J. (2008). Essential role for Nix in autophagic maturation of erythroid cells. Nature *454*, 232–235.

Sato, N., Patel, H.J., Waldmann, T.A., and Tagaya, Y. (2007). The IL-15/IL-15Ralpha on cell surfaces enables sustained IL-15 activity and contributes to the long survival of CD8 memory T cells. Proc. Natl. Acad. Sci. U S A *104*, 588–593.

Schweers, R.L., Zhang, J., Randall, M.S., Loyd, M.R., Li, W., Dorsey, F.C., Kundu, M., Opferman, J.T., Cleveland, J.L., Miller, J.L., and Ney, P.A. (2007). NIX is required for programmed mitochondrial clearance during reticulocyte maturation. Proc. Natl. Acad. Sci. U S A *104*, 19500–19505.

Secinaro, M.A., Fortner, K.A., Dienz, O., Logan, A., Murphy, M.P., Anathy, V., Boyson, J.E., and Budd, R.C. (2018). Glycolysis promotes caspase-3 activation in lipid rafts in T cells. Cell Death Dis. *9*, 62.

Shefa, U., Jeong, N.Y., Song, I.O., Chung, H.-J., Kim, D., Jung, J., and Huh, Y. (2019). Mitophagy links oxidative stress conditions and neurodegenerative diseases. Neural Regen. Res. *14*, 749–756.

Shimomura, Y., Honda, T., Shiraki, M., Murakami, T., Sato, J., Kobayashi, H., Mawatari, K., Obayashi, M., and Harris, R.A. (2006). Branched-chain amino acid catabolism in exercise and liver disease. J. Nutr. *136* (*1, Suppl*), 250S–253S.

Stemmer, M., Thumberger, T., Del Sol Keyer, M., Wittbrodt, J., and Mateo, J.L. (2015). CCTop: An intuitive, flexible and reliable CRISPR/Cas9 target prediction tool. PLoS ONE *10*, e0124633.

Sugiura, A., and Rathmell, J.C. (2018). Metabolic barriers to T cell function in tumors. J. Immunol. *200*, 400–407.

Tata, A., and Brossay, L. (2018). Role of the KLRG1 pathway in the immune response. J. Immunol. *200*, 49.9.

van der Windt, G.J.W., Everts, B., Chang, C.H., Curtis, J.D., Freitas, T.C., Amiel, E., Pearce, E.J., and Pearce, E.L. (2012). Mitochondrial respiratory capacity is a critical regulator of CD8+ T cell memory development. Immunity *36*, 68–78.

van der Windt, G.J.W., O'Sullivan, D., Everts, B., Huang, S.C., Buck, M.D., Curtis, J.D., Chang, C.H., Smith, A.M., Ai, T., Faubert, B., et al. (2013). CD8 memory T cells have a bioenergetic advantage that underlies their rapid recall ability. Proc. Natl. Acad. Sci. U S A *110*, 14336–14341.

van Duikeren, S., Fransen, M.F., Redeker, A., Wieles, B., Platenburg, G., Krebber, W.J., Ossendorp, F., Melief, C.J., and Arens, R. (2012). Vaccine-induced effector-memory CD8$^+$ T cell responses predict therapeutic efficacy against tumors. J. Immunol. *189*, 3397–3403.

Vantaku, V., Donepudi, S.R., Ambati, C.R., Jin, F., Putluri, V., Nguyen, K., Rajapakshe, K., Coarfa, C., Battula, V.L., Lotan, Y., and Putluri, N. (2017). Expression of ganglioside GD2, reprogram the lipid metabolism and EMT phenotype in bladder cancer. Oncotarget *8*, 95620–95631.

Vockley, J., Mohsen al-W, A., Binzak, B., Willard, J., and Fauq, A. (2000). Mammalian branched-chain acyl-CoA dehydrogenases: molecular cloning and characterization of recombinant enzymes. Methods Enzymol. *324*, 241–258.

Voehringer, D., Koschella, M., and Pircher, H. (2002). Lack of proliferative capacity of human effector and memory T cells expressing killer cell lectinlike receptor G1 (KLRG1). Blood *100*, 3698–3702.

Walter, D.M., Venancio, O.S., Buza, E.L., Tobias, J.W., Deshpande, C., Gudiel, A.A., Kim-Kiselak, C., Cicchini, M., Yates, T.J., and Feldser, D.M. (2017). Systematic in vivo inactivation of chromatin regulating enzymes identifies Setd2 as a potent tumor suppressor in lung adenocarcinoma. Cancer Res. *77*, 1719–1729.

Watkins, P.A., Lu, J.-F., Steinberg, S.J., Gould, S.J., Smith, K.D., and Braiterman, L.T. (1998). Disruption of the *Saccharomyces cerevisiae FAT1* gene decreases very long-chain fatty acyl-CoA synthetase activity and elevates intracellular very long-chain fatty acid concentrations. J. Biol. Chem. *273*, 18210–18219.

Weant, A.E., Michalek, R.D., Khan, I.U., Holbrook, B.C., Willingham, M.C., and Grayson, J.M. (2008). Apoptosis regulators Bim and Fas function concurrently to control autoimmunity and CD8$^+$ T cell contraction. Immunity *28*, 218–230.

Witte, I., and Horke, S. (2011). Assessment of endoplasmic reticulum stress and the unfolded protein response in endothelial cells. Methods Enzymol. *489*, 127–146.

Xu, X., Araki, K., Li, S., Han, J.H., Ye, L., Tan, W.G., Konieczny, B.T., Bruinsma, M.W., Martinez, J., Pearce, E.L., et al. (2014). Autophagy is essential for effector CD8(+) T cell survival and memory formation. Nat. Immunol. *15*, 1152–1161.

Xu, A., Bhanumathy, K.K., Wu, J., Ye, Z., Freywald, A., Leary, S.C., Li, R., and Xiang, J. (2016). IL-15 signaling promotes adoptive effector T-cell survival and memory formation in irradiation-induced lymphopenia. Cell Biosci. *6*, 30.

Youngblood, B., Hale, J.S., Kissick, H.T., Ahn, E., Xu, X., Wieland, A., Araki, K., West, E.E., Ghoneim, H.E., Fan, Y., et al. (2017). Effector CD8 T cells dedifferentiate into long-lived memory cells. Nature *552*, 404–409.

Yu, D., and Ye, L. (2018). A portrait of CXCR5$^+$ follicular cytotoxic CD8$^+$ T cells. Trends Immunol. *39*, 965–979.

Yuzefpolskiy, Y., Baumann, F.M., Kalia, V., and Sarkar, S. (2015). Early CD8 T-cell memory precursors and terminal effectors exhibit equipotent *in vivo* degranulation. Cell. Mol. Immunol. *12*, 400–408.

Zhou, X., and Xue, H.H. (2012). Generation of memory precursors and functional memory CD8+ T cells depends on TCF-1 and LEF-1. J. Immunol. *15*, 2722–2726.

STAR★METHODS

KEY RESOURCES TABLE

REAGENT or RESOURCE	SOURCE	IDENTIFIER
Antibodies		
APC anti-mouse CD3 antibody	Biolegend	RRID: AB_2561456; Cat#100236
APC anti-mouse CD8a antibody	Biolegend	RRID: AB_312751; Cat#100712
Pacific Blue anti-mouse CD8a antibody	Biolegend	RRID: AB_493425; Cat#100725
APC/Fire 750 anti-mouse CD8a antibody	Biolegend	RRID: AB_2572113; Cat#100766
FITC anti-mouse/human CD44 antibody	Biolegend	RRID: AB_312957; Cat#103006
APC anti-mouse/human CD44 antibody	Biolegend	RRID: AB_312963; Cat#103012
APC/Fire 750 anti-mouse/human CD44 antibody	Biolegend	RRID: AB_2616727; Cat#103062
PE/Cy7 anti-mouse CD62L antibody	Biolegend	RRID: AB_313103; Cat#104418
APC/Fire 750 anti-mouse CD62L antibody	Biolegend	RRID: AB_2629772; Cat#104450
PerCP/Cy5.5 anti-mouse CD43 Activation-Associated Glycoform antibody	Biolegend	RRID: AB_2286556; Cat#121224
PE anti-mouse CD127 (IL-7Rα) Antibody	Biolegend	RRID: AB_1937251; Cat#135010
Anti-mouse CD127 PE-Cy5 50 ug antibody	Thermo Fisher Scientific	RRID: AB_468792; Cat#15-1271-81
FITC Mouse Anti-Mouse CD45.2	BD PharMingen	RRID: AB_395041; Cat#553772
PE/Cy7 anti-mouse CD366 (Tim-3) Antibody	Biolegend	RRID: AB_2632733; Cat#134009
Mouse TCF7/TCF1 Alexa Fluor® 647-conjugated Antibody	R&D Systems	Cat#FAB8224R
PE/Cy7 anti-mouse/human KLRG1 (MAFA) antibody	Biolegend	RRID: AB_2561736; Cat#138416
Brilliant Violet 605 anti-mouse CD185 (CXCR5) Antibody	Biolegend	RRID: AB_2562208; Cat#145513
PE/APC anti-mouse H-2K(b) SIINFEKL antibody (Ova_tetramer)	Baylor College of Medicine MHC Tetramer Production Core	Cat#16114
FITC Annexin V	BD PharMingen	Cat#51-65874X
CD3e antibody	BD Biosciences	RRID: AB_394591; Cat#553058
Ultra-LEAF Purified anti-mouse CD3 antibody	Biolegend	RRID: AB_2616673; Cat#100359
CD28 antibody	BD Biosciences	RRID: AB_394763; Cat#553294
Anti-mouse HIF-1 alpha Antibody	Novus Biologicals	RRID: AB_10001045; Cat#NB100-449
Anti-mouse TFAM antibody	Santa Cruz Biotechnology	RRID: AB_10610743; Cat#sc-166965
Anti-mouse ACADSB antibody	Novus Biologicals	Cat#NBP1-97833
Chemicals, Peptides, and Recombinant Proteins		
CAY10585	Cayman Chemical	Cat#*934593-90-5*
Ovalbumin	Sigma-Aldrich	Cat#A7641
N-Acetyl-L-Cysteine (NAC)	Sigma-Aldrich	Cat#A7250
Hexadimethrine Bromide (polybrene)	Sigma-Aldrich	Cat#H9268
Etomoxir	Sigma-Aldrich	Cat#E1905
FCCP	Sigma-Aldrich	Cat#C2920
Mouse IL-15	Biolegend	Cat#566304
Critical Commercial Assays		
ATP Determination kit	Molecular Probes	Cat#A22066
Mouse IL-2 ELISA MAX Standard	Biolegend	Cat#431002
Mouse IFNg ELISA MAX Standard	Biolegend	Cat#430802
Mouse TNF ELISA Set	BD Biosciences	Cat#555268
MitoSOX Red mitochondrial superoxide indicator	Invitrogen	Cat#M36008
Mitotracker Green FM	Invitrogen	Cat#M7514
JC-1 dye	Invitrogen	Cat#T3168

(*Continued on next page*)

Continued

REAGENT or RESOURCE	SOURCE	IDENTIFIER
Seahorse Xfe96 Flux assay kit	Agilent Technologies	Cat#101085-004
Mouse DNA Damage Analysis Kit	Detroit R&D	Cat#DD2M
Experimental Models: Cell Lines		
NIH 3T3	CLS	CVCL_0594
293T	ATCC	CVCL_0063
BHK-21	CLS	CVCL_1915
Experimental Models: Organisms/Strains		
Mouse: C57BL/6J	The Jackson Laboratory	IMSR_JAX:000664
Mouse: NIX$^{f/f}$	Diwan et al., 2007	N/A
Mouse: B6.Cg-Tg(Lck-cre)548Jxm/J	The Jackson Laboratory	IMSR_JAX:003802
Mouse: C57BL/6-Tg(TcraTcrb)1100Mjb/J	The Jackson Laboratory	IMSR_JAX:003831
Mouse: B6.SJL-Ptprc^{a} Pep3^{b}/BoyJ, Pep Boy, B6 Cd45.1	The Jackson Laboratory	IMSR_JAX:002014
Oligonucleotides		
Primers for *18S*, see Table S1	This paper	N/A
Primers for *Nix*, see Table S1	This paper	N/A
Primers for *Bnip3*, see Table S1	This paper	N/A
Primers for *Il-15rα*, see Table S1	This paper	N/A
Primers for *Foxo1*, see Table S1	This paper	N/A
Primers for *Tcf7*, see Table S1	This paper	N/A
Primers for *Blimp-1*, see Table S1	This paper	N/A
Primers for *Tfam*, see Table S1	This paper	N/A
Primers for *Fasn*, see Table S1	This paper	N/A
Primers for *Bckdk*, see Table S1	This paper	N/A
Primers for *Acadl*, see Table S1	This paper	N/A
Primers for *Acadsb*, see Table S1	This paper	N/A
Primers for *Acadm*, see Table S1	This paper	N/A
Primers for *Acads*, see Table S1	This paper	N/A
Primers for *Acad11*, see Table S1	This paper	N/A
Primers for *Atp5b*, see Table S1	This paper	N/A
Primers for *Atp5f1*, see Table S1	This paper	N/A
Primers for *Ehhadh*, see Table S1	This paper	N/A
Primers for *Gls*, see Table S1	This paper	N/A
Primers for *Glut1*, see Table S1	This paper	N/A
Primers for *Prkaa1*, see Table S1	This paper	N/A
Primers for *Pdha1*, see Table S1	This paper	N/A
Primers for *Pink1*, see Table S1	This paper	N/A
Primers for *Parkin*, see Table S1	Bian et al., 2012	N/A
Primers for *Caspase-3*, see Table S1	This paper	N/A
Primers for *Hif1α*, see Table S1	This paper	N/A
Primers for *Hif1α^{2nd}*, see Table S1	This paper	N/A
Primers for *Acadsb*, see Table S1	This paper	N/A
Software and Algorithms		
FlowJo	FlowJo, LLC	SCR_008520
Prism	GraphPad Software	SCR_002798
SoftWorx	Applied Precision	N/A
Seahorse Wave	Agilent Technologies	SCR_014526

(*Continued on next page*)

Continued

REAGENT or RESOURCE	SOURCE	IDENTIFIER
Recombinant DNA		
psPAX	Didier Trono Lab	Addgene_12260
pMD2.G	Didier Trono Lab	Addgene_12259
LentiCRISPRv2 plasmid	Walter et al., 2017	Addgene_82416

LEAD CONTACT AND MATERIALS AVAILABILITY

Further information and requests for resources and reagents should be directed to and will be fulfilled by the Lead Contact, Min Chen (minc@bcm.edu). All unique/stable reagents generated in this study are available from the Lead Contact with a completed Materials Transfer Agreement.

EXPERIMENTAL MODEL AND SUBJECT DETAILS

Animals

All mice used in the study were bred at Baylor College of Medicine in agreement with the guidelines of the Institutional Animal Care and Use Committee. For the generation of T/NIX$^{-/-}$ mice, B6.Cg-Tg(Lck-cre)548Jxm/J mice (LCK^{Cre} mice; The Jackson Laboratory) were cross-bred with NIX$^{f/f}$ mice (Diwan et al., 2007). In T/NIX$^{-/-}$ mice, NIX was flanked with LoxP sequences and expression of Cre was regulated under Lymphocyte protein tyrosine kinase (Lck) promoter. Other strains of mice used in the study were: C57BL/6J (WT or CD45.2^{+} mice), B6.SJL-Ptprc^{a} Pep3^{b}/BoyJ (CD45.1^{+} mice) and C57BL/6-Tg(TcraTcrb)1100Mjb/J (OT-I mice) mice, all of which were purchased from The Jackson Laboratory. OT-I T/NIX$^{-/-}$ mice were generated by cross-breeding OT-I and T/NIX$^{-/-}$ mice, and OT-I Lck^{Cre} mice were generated by cross-breeding OT-I and Lck^{Cre} mice. Experiments were conducted with age-matched (mice aged 6 to 16 week old were used) and gender-matched (both male and female mice were used) mice. In all experiments, WT or OT-I or OT-I Lck^{Cre} mice were used as controls.

Cell lines and primary cell cultures

Splenocytes harvested from the mice were cultured in T cell media [RPMI 1640 (Corning)+10% FBS (GIBCO)+1X antibiotic-antimycotic (GIBCO)]. BHK-21, 293T and 3T3 cells were maintained in DMEM/High-glucose (HyClone)+10% FBS (GIBCO)+1X antibiotic-antimycotic (GIBCO).

METHOD DETAILS

Virus, immunization and infection

Vesicular Stomatitis Virus co-expressing Ovalbumin (VSV-Ova) was propagated in BHK-21 cells at an MOI of 0.01, and concentrated at 15,000 rpm in an SW28 (Beckman) rotor for 5 hours. Viral titer was determined using plaque assay on BHK-21 cells. Gender- and age-matched mice were immunized with 10^4 PFU of VSV-Ova via tail vein injection. For infection experiments, mice were injected with 10^6 PFU of VSV-Ova via tail-vein injection. In all injections, VSV-Ova was suspended in sterile 1X DPBS (GIBCO).

Flow cytometry

Ova-specific effector memory CD8+ T cells and Ova-specific activated CD8+ T cells were pre-treated with FcRγII/III (Fc blocker) and IgG$_{2b}$ anti-mouse CD16/CD32 antibodies, then stained with the following anti-mouse fluorescent-conjugated antibodies: CD3 (Biolegend#100236), CD8 (Biolegend #100712/#100725), CD44 (Biolegend#103006/#103012/#103062), CD62L (Biolegend#104418), CD43 (Biolegend #121224), CD127 (Thermo Fisher Scientific#15-1271-81/Biolegend#135010), KLRG1 (Biolegend#138416), CD45.2 (BD PharMingen#553772), CXCR5 (Biolegend#145513), TIM3 (Biolegend#134009), TCF7 (R&D Systems # FAB8224R) and SIINFEKL peptide-specific Ova_tetramer (Baylor College of Medicine's MHC tetramer production facility #16114) and finally analyzed on BD FACSCantoII (BD Biosciences) or BD LSRII (BD Biosciences). For MitoTracker Green staining, Ova-specific effector memory CD8+ T cells were stained with 100nM MitoTracker Green FM (Invitrogen) and analyzed on BD FACSCantoII. For MitoSOX Red staining, Ova-specific CD8+ T cells were stained with 5uM MitoSOX Red (Molecular Probes) and analyzed on BD FACSCantoII. For CytoID staining, Ova-specific effector memory CD8+ T cells or naive CD8+ T cells were pre-treated with 10uM chloroquine for 2 hours to inhibit autophagosomal degradation, followed by detection of autophagy flux using Cyto-ID autophagy detection kit (Enzo) according to manufacturer's instructions. For experiments involving CFSE staining, cells were labeled with 5uM of CFSE prior to stimulation with 1ug/mL anti-mouse CD3 (BD Biosciences#553058) and 1ug/mL anti-mouse CD28 (BD Biosciences#553294) antibodies or stained with 5uM of CFSE prior to the adoptive transfer. Cells not stained with CFSE served as unstained control; and CFSE stained cells which were either not stimulated with CD3/CD28- amtibodies or not adoptively transferred into the recipients served as non-activated control. All analyses were done using FlowJo software.

CD8$^+$ population enrichment and cell sorting

For enrichment with CD8$^+$ population, cells were labeled with CD8a microbeads (Miltenyi) and magnetically sorted using autoMACS (Miltenyi). CD8$^+$ population was then pre-treated with FcRγII/III (Fc blocker) and IgG$_{2b}$ anti-mouse CD16/CD32 antibodies, and stained with fluorescent-conjugated antibodies against mouse- CD8 (Biolegend#100712/#100725/#100766), CD44 (Biolegend #103006/Biolegend #103012/Biolegend #103062), CD62L (Biolegend # 104418/#104450), CD43 (Biolegend#121224), CD127 (Thermo Fisher#15-1271-81/Biolegend #135010), KLRG1 (Biolegend#138416), CXCR5 (Biolegend#145513), TIM3 (Biolegend#134009), TCF7 (R&D Systems#FAB8224R) and Ova_tetramer (Baylor College of Medicine's MHC tetramer production facility#16114 or #19020) for Ova-EM, Ova-CM, naive CD8$^+$ and Ova- CD8$^+$ MPEC. In addition, Ghost Dye Violet 510 (Tonbo #13-0870) or NucBlue DAPI (Invitrogen #R37606) were also used to selectively sort live cells. In those cases, Ghost Dye Violet 510$^-$ or NucBlue DAPI$^-$ populations were further sub-gated into Ova-EM, Ova-CM, naive CD8$^+$ and Ova-CD8$^+$ MPEC. Stained cells were sorted on BD FACSAriaII (BD Biosciences). Typical purity after cell sorting was > 95%.

Effector memory formation in CD8$^+$ T cells *in vitro*

Splenocytes were pulsed with Ovalbumin and cultured in T cell media, 55uM of 2-Mercaptoethanol (GIBCO) and 100units/mL IL-2 for 3 days, after which the cells were washed with 1X PBS (containing 2% adult serum) and cultured in T cell media and 20ng/mL mouse IL-15 (Biosource/Biolegend) for five additional days. For effector memory formation in case of extracellular flux analysis and CRISPR/Cas9-mediated gene knockout experiments, splenocytes from OT-I (OT-I WT) or OT-I x LCK^{Cre} (OT-I WT) or OT-I x NIX$^{f/f}$ (OT-I WT) and OT-I x LCK^{Cre} x NIX$^{f/f}$ (OT-I T/NIX$^{-/-}$) mice were used.

For experiments where gene expression of NIX was measured, CD8$^+$ T cells from naive OT-I mice were stimulated with either 1ug/mL each of anti-CD3 or anti-CD3/CD28 antibodies for 3 days. CD8$^+$ T cells were then washed and 20ng/mL of fresh IL-15 was added.

Adoptive transfer

For memory recall experiments (flow cytometry and ELISA for IFN-γ and IL-2), equal number of sorted Ova-specific effector memory CD8$^+$ T cells (CD45.2$^+$), that were formed either *in vivo* or *in vitro*, were resuspended in sterile 1X DPBS and injected into naive CD45.1$^+$ mice via tail vein injection. In case of experiments, where protection against VSV-Ova infection was assessed (viral titer and ELISA for IFN-γ), equal number of cells on day 8 of *in vitro* formation of effector memory were injected into naive CD45.1$^+$ mice via tail vein injection. Recipient naive CD45.1$^+$ mice were challenged with 10^4 PFU (memory recall experiments) or 10^6 PFU (infection experiments) of VSV-Ova via tail vein injection 24 hours later. 48 hours after VSV-Ova challenge/infection, mice were sacrificed and their peripheral organs or blood were harvested for further analysis. For CFSE proliferation assay, Ova-specific effector memory CD8$^+$ T cells were labeled with 5uM CFSE before adoptive transfer.

Quantitative PCR and PCR array of metabolic genes

To assess the expression of genes, Ova-specific effector memory CD8$^+$ T cells (Ova-EM) or Ova-specific central memory CD8$^+$ T cells (Ova-CM) or Ova-specific memory precursor effector cells (Ova-CD8$^+$ MPECs) or Ova-specific reactivated Ova-EM were sorted and total RNA was extracted using Direct-zol RNA microprep kit (Zymo Research). Extracted RNA was then reverse-transcribed into cDNA using SuperScript IV VILO Master Mix with ezDNase Enzyme kit (Invitrogen). Quantitative PCR was performed using iTaq Universal Probes Supermix (Bio-Rad) with primers targeting mouse *18S* (Forward: 5′-ATTGACGGAAGGGCACCAC-3′; Reverse: 5′-TCTAAGAAGTTGGGGGACGC-3′), *Nix* (Forward: 5′- GAGCCGGATACTGTCGTCCT −3′; Reverse: 5′- CAATATAGATG CCGAGCCCCA −3′), *Bnip3* (Forward: 5′- AACAGCACTCTGTCTGAGGAA −3′; Reverse: 5′- TGTCAGACGCCTTCCAATGT −3′), *IL-15Rα* (Forward: 5′- ACATCGGTCCTCTTGGTTGG −3′; Reverse: 5′- CGTGTGGTTAGGCTCCTGTG −3′), *Foxo1* (Forward: 5′-CAC ACATCTGCCATGAACCG-3′; Reverse: 5′-GGTGGAGGACACCCATCCTA-3′), *Tcf7* (Forward: 5′-CGGAAAGAAGAAGAGGCGGT-3′; Reverse: 5′-CTGTCATCGGAAGGAACGGG-3′), *Blimp-1* (Forward: 5′- GGACTGGGTGGACATGAGAG −3′; Reverse: 5′- TTCACGTA GCGCATCCAGTT −3′), *Tfam* (Forward: 5′- TAGGCACCGTATTGCGTGAG −3′; Reverse: 5′- GACAAGACTGATAGACGAGGGG-3′), *Fasn* (Forward: 5′-TTGACGGCTCACACACCTAC-3′; Reverse: 5′-TTGTGGTAGAAGGACACGGC-3′), *Bckdk* (Forward: 5′-TTCCCCTT CATTCCCATGCC-3′; Reverse: 5′-CCGTAGGTAGACATCCGTGC-3′), *Pink1* (Forward: 5′- GTGGGACTCAGATGGCTGTC-3′; Reverse: 5′- GCACATTTGCAGCTAAGCGT-3′), *Parkin* (Forward: 5′- CCAAACCGGATGAGTGGTGAGTGC-3′; Reverse: 5′- ACACGG CAGGGAGTAGCCAAGTTG-3′) and *Caspase-3* (Forward: 5′- AGCTGGACTGTGGCATTGAG-3′; Reverse: 5′- CCACGACCCGTCC TTTGAAT-3′).

For PCR array of metabolic genes, primers targeting mouse *Acadl* (Forward: 5′- GTGTATCGGTGCCATAGCCA-3′; Reverse: 5′-AGGCAGAAATCGCCAACTCA-3′), *Acadsb* (Forward: 5′–3′; Reverse: 5′–3′), *Acadm* (Forward: 5′-TTCGAAGACGTCAGA GTGCC-3′; Reverse: 5′-GCTCCACTAGCAGCTTTCCA-3′), *Acads* (Forward: 5′-TTGCCGAGAAGGAGTTGGTC-3′; Reverse: 5′-AGG TAATCCAAGCCTGCACC-3′), *Acad11* (Forward: 5′-CGCCTTGGACCTGGAAGAAT-3′; Reverse: 5′-TTCAAGGTCAGCAAGCGG AT-3′), *Atp5b* (Forward: 5′-GTTGGTCCTGAGACCTTGGG-3′; Reverse: 5′-TCCGATTTTCCCACCCTTGG-3′), *Atp5f1* (Forward: 5′-TCCAGGGGTATTACAGGCAAC-3′; Reverse: 5′-CAGCCCAAGACGCACTTTTC-3′), *Ehhadh* (Forward: 5′-CGGTCAATGCCAT CAGTCCA-3′; Reverse: 5′-AGCACCTGCACAGAAGTTGT-3′), *Gls* (Forward: 5′-CCGCGGGCGACAATAAAATAA-3′; Reverse:

5′-GCATGACACCATCTGACGTT-3′), *Glut1* (Forward: 5′-ATAGTTACAGCGCGTCCGTT-3′; Reverse: 5′-AGAGACCAAAGCGTG GTGAG-3′), *Prkaa1* (Forward: 5′-GTGAAGATCGGCCACTACATCC-3′; Reverse: 5′-GGCTTTCCTTTTCGTCCAACC-3′), *Pdha1* (Forward: 5′-GCCACCCTGAACCTGAGAAA-3′; Reverse: 5′-GCGATACATCATTACATCCACG-3′) were used

Quality control on all the primers was performed in-house to ensure band specificity, accuracy and reliability. Data were normalized to that for *18S* and expressed as relative abundance via $2^{-\Delta\Delta CT}$ method, where CT is the threshold cycle. Unless specified in the figure legends, final results were represented relative to Day 0 time point (in case of NIX expression) or WT or WT (+DMSO) (in case of expression all other genes), as indicated in respective figures.

Measurement of apoptosis in Ova-CD8$^+$ MPECs and Ova-EM

Splenocytes were harvested from WT and T/NIX$^{-/-}$ mice 20 days after immunization with 10^4 PFU of VSV-Ova, pre-treated with FcRγII/III (Fc blocker) and IgG_{2b} anti-mouse CD16/CD32 antibodies, and stained with the following anti-mouse fluorescent-conjugated antibodies: CD8 (Biolegend#100725), CD44 (Biolegend#103062), CD62L (Biolegend#104418), CD43 (Biolegend#121224), CD127 (Biolegend#135010) and SIINFEKL peptide-specific Ova_tetramer (Baylor College of Medicine's MHC tetramer production facility#16114). Next, surface stained splenocytes were washed with 1X PBS, incubated in Annexin V (BD PharMingen #51-65874X) at room temperature (away from light) for 20 mins and analyzed on BD FACSCantoII within 1 hour. Percentage of Annexin V$^+$ population in Ova-CD8$^+$ MPECs and Ova-EM represented cells undergoing apoptosis.

Immunocytochemistry

Ova-specific effector memory CD8$^+$ T cells, Ova-specific central memory CD8$^+$ T cells or naive CD8$^+$ T cells formed *in vivo* in WT and T/NIX$^{-/-}$ mice were sorted 30 days after VSV-Ova immunization, treated with 10uM chloroquine for 2 hours to inhibit autophagosomal degradation, and applied to slides by cytospin. The cells were then fixed, permeabilized and incubated with mouse anti-COX IV (Invitrogen#459600) and rabbit anti-LC3 (Abgent#AP1801a) to stain mitochondria and autophagosomes respectively. This was followed by staining with Alexa Fluor conjugated secondary antibodies (Molecular Probes) and examination of slides under 100X objective (U PlanS-Apo/1.4, oil immersion) of deconvolution microscope (GE Healthcare Deltavision LIVE High Resolution) using SoftWoRx acquisition software. The Pearson coefficiency of correlation for LC3 and COX IV co-localization was determined using SoftWoRx software (Applied Precision).

Measurement of mitochondrial membrane depolarization

Splenocytes were harvested from WT and T/NIX$^{-/-}$ mice 20 days after immunization with 10^4 PFU of VSV-Ova, pre-treated with FcRγII/III (Fc blocker) and IgG_{2b} anti-mouse CD16/CD32 antibodies, and stained with the following anti-mouse fluorescent-conjugated antibodies: CD8 (Biolegend#100725) and SIINFEKL peptide-specific Ova_tetramer (Baylor College of Medicine's MHC tetramer production facility#16114). Next, surface stained splenocytes were washed and incubated in 2.5ug/mL of JC-1 in 37C for 30 mins. Splenocytes were then washed and analyzed on BD LSRII (BD Biosciences). Mitochondrial membrane depolarization was indicated by geometric MFI of green fluorescence corresponding to JC-1 monomers in Ova-specific CD8$^+$ T cells.

Mitochondrial DNA damage assay

Mitochondrial DNA damage was assessed using mouse DNA Damage Analysis Kit (Detroit R&D#DD2M) according to manufacturer's instructions. Briefly, 100,000 sorted Ova-specific CD8$^+$ T cells from day 20 p.i. mice were lysed in lysis buffer (5M sodium chloride, 1M tris, 0.5M EDTA, 10% SDS and 0.3mg/mL proteinase K) at 56C overnight, followed by heat inactivation of proteinase K at 95C for 10 mins. Cell lysates were then diluted 10X in nuclease-free water before using further. Samples (~5ng/uL DNA) were subjected to PCR reaction, after which 10X diluted PCR reaction product was subjected to real-time PCR. Final concentrations of damaged mitochondrial DNA were calculated from the 8.2kb standard curve plotted using 8.2kb real-time standard supplied with the kit.

Drug treatments

In experiments where CD8$^+$ effector memory was formed *in vivo*, NAC (1mg/mouse) was dissolved in sterile 1X DPBS and injected intraperitoneally (i.p.) once on days 13, 20 and 27 after immunization with VSV-Ova. In experiments, where CD8$^+$ effector memory was formed *in vitro*, 100uM of NAC (dissolved in sterile 1X DPBS) (Sigma Aldrich#A7250) or 3uM of CAY10585 (dissolved in DMSO) (Cayman Chemical#*934593-90-5*) or 10nM Oligomycin (dissolved in DMSO) or 100nM rapamycin (dissolved in DMSO) was added once on day 4 of culture.

Intracellular staining

Surface stained Ova-specific effector memory CD8$^+$ T cells were fixed and permeabilized with Cytofix/Cytoperm kit (BD Biosciences), followed by staining with rabbit anti-mouse HIF1α antibody (Novus Biologicals#nb100-449) or mouse anti-mouse TFAM (Santa Cruz Biotechnology#sc-166965) at 4°C for 1 hour. This was followed by staining with Alexa Fluor conjugated secondary antibodies (Molecular Probes) at 4°C for 1 hour. In case of intracellular staining of IL-2 and IFN-γ, splenocytes harvested from CD45.1$^+$ mice were pre-treated with FcRγII/III (Fc blocker) and IgG_{2b} anti-mouse CD16/CD32 antibodies, then stained with anti-mouse CD8 (Biolegend#100725), anti-mouse CD45.2 (BD PharMingen#561096) and anti-mouse Ova_tetramer before intracellular staining. Surface stained splenocytes were then fixed and permeabilized with Cytofix/Cytoperm kit (BD Biosciences#554714), followed by

staining with anti-mouse IL-2 (BD PharMingen#554428) or anti-mouse IFN-γ (Biolegend# 505806). In case of intranuclear staining for TCF7, surface stained cells were fixed and permeabilized using Foxp3/Transcription factor staining buffer set (eBioscience#00-5523-00), followed by staining with anti-mouse TCF7/TCF1 antibody (R&D systems#FAB8224R). Stained cells were analyzed on BD FACSCantoII or BD LSRII.

CRISPR/Cas9-mediated deletion of Hif1α and Acadsb genes

For generation of single guide RNA specific to *Hif1α* and *Acadsb* genes (sgRNA-HIF1α, sgRNA-HIF1α^{2nd} and sgRNA-ACADSB), the 20-nucleotide target sequence was selected to precede 5′-NGG protospacer-adjacent motif (PAM) sequence using CRISPR/Cas9 design tool (Stemmer et al., 2015). Oligonucleotides were annealed and cloned into BsmBI-BsmBI sites in LentiCRISPRv2 plasmid (Addgene plasmid #82416). Unmodified LentiCRISPRv2 plasmid served as sgRNA-control in the study. The sgRNA sequences used in this study were: sgRNA-HIF1α (forward: 5′-CACCGAGCCCTAGATGGCTTTGTGA-3′ and reverse:5′-AAACTCACAAAGCCATC TAGGGCTC-3′), sgRNA-HIF1α^{2nd} (forward: 5′- CACCGAAGCATCCTGTACTGTCCTG-3′ and reverse:5′- AAACCAGGACAGTACAG GATGCTTC-3′) and sgRNA-ACADSB (forward: 5′- CACCGATGGATGAGAACTCAAAAA-3′ and reverse: 5′- AAACTTTTTGAGTTCT CATCCATC-3′).

To generate lentiviral particles, $8x10^6$ 293T cells were plated on a 10 cm dish, followed by co-transfection with 3ug LentiCRISPR plasmid (sgRNA- HIF1α, sgRNA-HIF1α^{2nd}, sgRNA-ACADSB or sgRNA-control), 1.33ug psPAX (Addgene plasmid #12260) and 0.6ug pMD2.G (Addgene plasmid #12259) by Lipofectamine 2000 transfection method (Invitrogen). The viral supernatant was collected after 48 and 72 hours, passed through 0.2um PES filter, pooled and frozen in −80C until further use.

In order to knock out *HIF1α* and *Acadsb* gene from $CD8^+$ T cells, splenocytes from OT-I (OT-I WT) or OT-I x LCK^{Cre} (OT-I WT) or OT-I x $NIX^{f/f}$ (OT-I WT) and OT-I x LCK^{Cre} x $NIX^{f/f}$ (OT-I T/$NIX^{-/-}$) mice were cultured in 24-well or 48-well plate pre-coated with 1ug/mL of anti-mouse CD3 antibody (Biolegend #100359) and anti-mouse CD28 antibody (BD Biosciences #553294) for 3 days. On day 3, cells were washed and 500,000 cells/well were plated in a flat-bottom 48-well plate in presence of 1mL of viral supernatant: sgRNA-HIF1α, sgRNA-HIF1α2^{nd}, sgRNA-ACADSB or sgRNA-control (unmodified LentiCRISPRv2 plasmid) and 10ug/ml polybrene (Sigma-Aldrich). The plated cells were then centrifuged at 1000 g for 90min in 32C, followed by incubation in 37C incubator for additional 2 hours. The viral supernatant was finally replaced by T cell media containing 20ng/mL IL-15 and cultured for 5 additional days for $CD8^+$ T cell effector memory formation.

Western blotting

For western blot studies to validate deletion of *Hif1α* via CRISPR-Cas9, cells were treated with 100uM of cobalt chloride for 6 hours prior to preparation of cell lysate. Cell lysate was prepared by incubating the cells in cell lysis buffer (50 mM HEPES, pH 7.4, 150 mM NaCl, 1 mM EDTA, 1% Triton X-100, and 1x protease inhibitor cocktail from Roche) for 60 mins on ice. Cell lysates were then heat denatured at 95°C for 6 minutes, quantified for total protein content by Bio-Rad Protein assay (Hercules, CA), electrophoretically resolved on SDS-PAGE, transferred onto PVDF membrane, and probed with primary antibodies (Novus Biologicals#NB100-449 for HIF1α, Novus Biologicals#NBP1-97833 for ACADSB and Santa Cruz Biotechnology#sc-47778 for β-actin) and horseradish peroxidase-conjugated secondary antibodies (Southern Biotechnology/Amersham). The blots were finally developed using Supersignal West Dura Extended Duration substrate (Thermo Scientific).

Viral titer assays

$1x10^6$ cells at the end of day 8 of *in vitro* $CD8^+$ T cell effector memory formation were resuspended in sterile 1X DPBS and injected into naive C57BL/6 mice via tail vein injection. 24 hours later, recipient mice were infected with 10^6 PFU of VSV-Ova via tail vein injection. 48 hours after infection, mice were sacrificed, and their brains were harvested. Brains were mashed in 1.5mL of T cell media, centrifuged at 12000 rpm for 3min in 4C and viral supernatant was collected and stored in −80C until further use. In case of viral titer determination in peripheral blood, blood was collected from heart of mice (immediately after euthanasia), allowed to clot at room temperature for 30 mins and centrifuged at 1000 g for 10 mins at 4°C. Supernatant (serum) was collected and stored in −80C until further use.

For plaque assay, 1.75×10^6 BHK-21 cells/well (plated a night before in 24-well plate), were incubated with diluted brain supernatant or 100uL serum for 4 hours in 37C (with intermittent shaking in between). Following this incubation, supernatant was aspirated and 50uL of plaque assay media (DMEM+ 2% FBS+1X antibiotic/antimycotic) was added, followed by addition of 2 mL overlay media (0.4% agarose+DMEM+2% FBS+1X antibiotic/antimycotic). The plate was then incubated in room temperature for 10 mins to solidify the overlay media. Following this incubation, cells were incubated in 37C for 24 hours. At the end of 24-hour incubation, the overlay media was gently removed, and wells were gently washed with 1X PBS once. The monolayer of BHK-21 cells was fixed with 4% paraformaldehyde solution for 30 minutes in room temperature, followed by gentle washing with sterile water once. This was followed by staining the monolayer with 0.2% Crystal Violet solution at room temperature for 30 mins. The wells were then gently washed with sterile water and number of colorless plaques were counted against violet background to get the viral titer.

Serum isolation and ELISA

After sacrificing the mice, as much blood as possible was collected from the heart. Blood was allowed to clot for 30 mins at room temperature after which it was centrifuged at 1000 g for 10 mins at 4°C. Supernatant was collected and stored in −80°C until further use. ELISA for mouse IL-2 and IFN-γ was then performed using ELISA Max kit (Biolegend) according to manufacturer's instructions.

Measurement of short/branched-chain fatty acids

Short/branched-chain fatty acids were extracted (Putluri et al., 2011a, 2014; Vantaku et al., 2017) by adding 100ul of acetonitrile: water (1:1). Cells were homogenized and supernatant was collected. To 40uL of supernatant, 20 ul of 200 mM 12C6-3NPH and 120 mM EDC.HCl were added and incubated for 30 min at 37°C. The resulting mixture was cooled and made up to 1.91 mL with 10% aqueous acetonitrile. 10 ul of the solution injected in to LC-MS. Mouse liver pool was used for quality control. ESI negative mode was used for the measurement. SRM was used and gradient Containing 0.1% formic acid in water (mobile phase A) and 0.1% formic acid in acetonitrile (mobile phase B). Separation of metabolites was performed on acquityUPLC HSS T3 1.8 um (2.1 × 100mM).The binary pump flow rate was 0.35 ml/min with a gradient starting 15% B at 0min, 50% at 10 min, 100% at 10.1min,15% at 13.1 min, reequilibration till the end of the gradient 17 min. 10 μL of sample was injected and analyzed using a 6490 triple quadrupole mass spectrometer (Agilent Technologies, Santa Clara, CA) coupled to a HPLC system (Agilent Technologies, Santa Clara, CA) via SRM. Source parameters were as follows: Gas temperature- 250°C; Gas flow- 14 l/min; Nebulizer - 20psi; Sheath gas temperature - 350°C; Sheath gas flow- 12 l/min; Capillary - 3000 V positive and 3000 V negative; Nozzle voltage- 1500 V positive and 1500 V negative. Approximately 8–11 data points were acquired per detected metabolite. The data points for each metabolite obtained were represented as fold change relative to WT.

Extracellular flux analysis (Seahorse assay)

Equal number of sorted Ova-specific effector memory $CD8^+$ T cells were plated in microplate pre-coated with Cell Tak. Extracellular flux analysis was performed in Seahorse XFe96 Analyzer (Agilent). For OCR measurement related to measuring long-chain fatty acid oxidation, cells were plated in bicarbonate-free RPMI (Agilent) with 20mM glucose, 1X glutamax and 1X sodium pyruvate. Mitochondrial spare respiratory capacity (SRC) was calculated as the mean difference between OCR after FCCP injection and basal OCR (before Oligomycin injection). Long-chain fatty acid oxidation was calculated as the difference between mean OCR after injection of FCCP and mean OCR after injection of etomoxir (200uM final concentration). Long-chain fatty acid oxidation was plotted as fold-change in OCR relative to WT (+DMSO). Oligomycin, FCCP, Rotenone and Antimycin A were injected at final concentrations of 1uM, 2uM, 100nM and 1uM respectively.

For OCR measurement related to measuring short/branched-chain fatty acid oxidation, cells were plated in Krebs-Henseleit Buffer (KHB) with 20mM glucose, 1X glutamax and 1X sodium pyruvate. BCAA (final concentration of 1-1.5 mg/mL leucine, 1-1.5 mg/mL isoleucine and 0.4-0.6 mg/mL valine) was injected during the measurement of OCR. Short/branched-chain fatty acid oxidation was calculated as:

Mean OCR after injection of BCAA/ Mean OCR before injection of BCAA.

ATP assay

Sorted Ova-specific effector memory $CD8^+$ T cells were lysed in lysis buffer (150mM sodium chloride, 1mM EDTA, 50mM HEPES adjusted to pH 7.4, 10% glycerol and 1% NP40) for 1 hour on ice. The cell lysate was then centrifuged at 16000xg for 10 minutes, and supernatant collected and used for ATP assay. ATP assay was performed using ATP Determination kit (Invitrogen#A22066) according to manufacturer's instructions. Results were represented as values relative to WT or WT (+DMSO), as applicable to relevant figures.

QUANTIFICATION AND STATISTICAL ANALYSIS

Data were presented as mean ± SEM and p values were calculated using two-tailed Student's t test, one-way or two-way ANOVA with Bonferroni's posttests as indicated in the figure legends. Statistical analyses were done using GraphPad Prism software, assuming normal data distribution and equal sample variance. For measurement of fatty acids, the data was log2-transformed and normalized with internal standard per-sample. Number of mice used in each group in the study was consistent with previously published studies of similar nature. Any statistical difference < 0.05 was considered as significant and is indicated in figure legends.

DATA AND CODE AVAILABILITY

This study did not generate any unique datasets or code.

Cell Reports, Volume *29*

Supplemental Information

NIX-Mediated Mitophagy Promotes Effector Memory Formation in Antigen-Specific $CD8^+$ T Cells

Shubhranshu S. Gupta, Robert Sharp, Colby Hofferek, Le Kuai, Gerald W. Dorn II, Jin Wang, and Min Chen

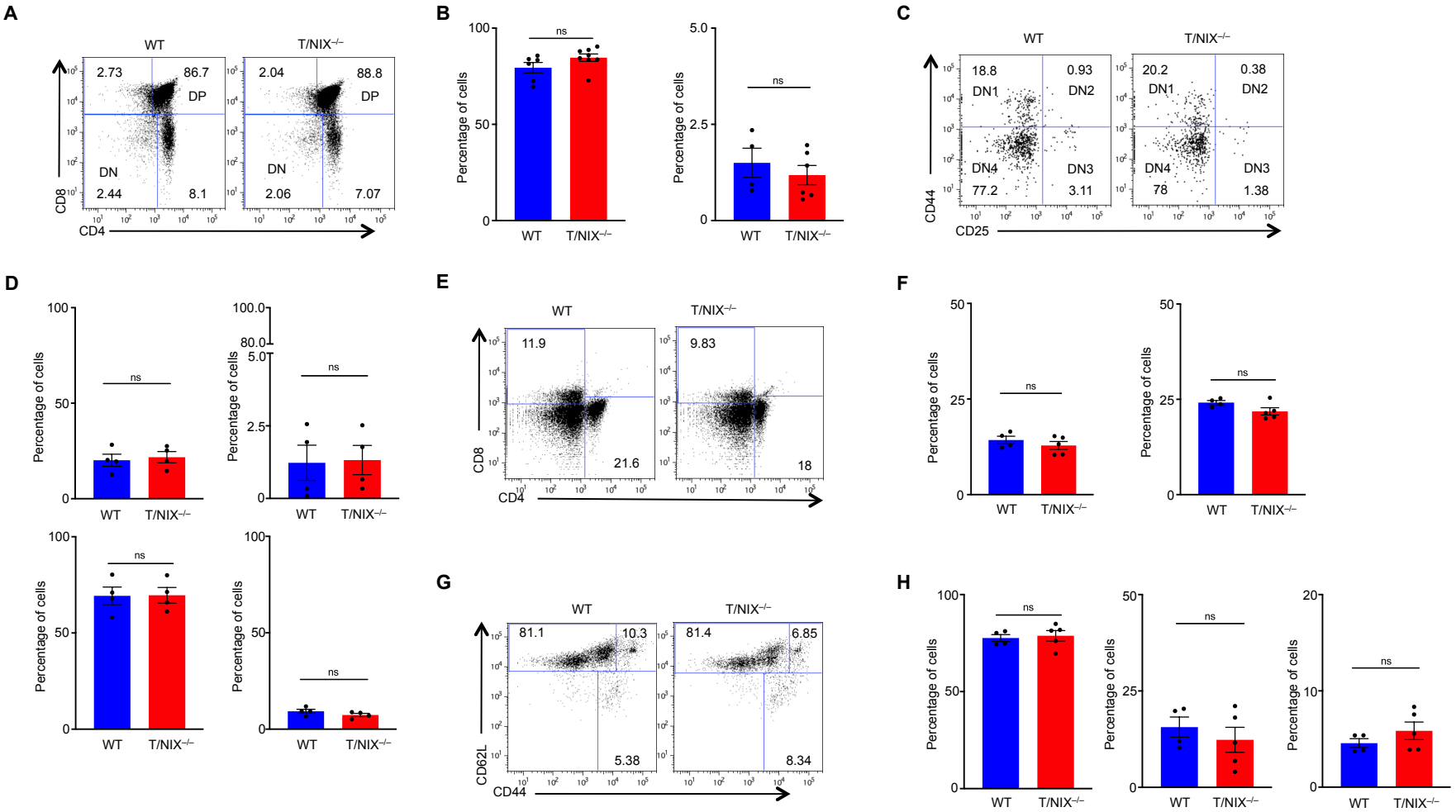

Figure S1. Deletion of NIX in T Cells Does Not Alter the Development of CD4⁺ and CD8⁺ T Cells, **Related to Figure 1. (A)** Representative dot plot showing percentage of populations corresponding to double negative (DN) and double positive (DP) stages of T cell development in Thymus in wild-type and T/NIX$^{-/-}$ mice. **(B)** Mean percentage of double positive (left) and double negative (DN) (right) from the experiment in **(A)**. **(C)** Representative dot plot showing percentage of DN1 (CD44^{+}CD25^{-}), DN2 (CD44^{+}CD25^{+}), DN3 (CD44^{-}CD25^{+}) and DN4 (CD44^{-}CD25^{-}) populations in Thymus from wild-type and T/NIX$^{-/-}$ mice. **(D)** Mean percentage of DN1 (top left), DN2 (top right), DN3 (bottom right) and DN4 (bottom left) populations from the corresponding gates in panel **(C)**. **(E)** Representative dot plot showing percentage of CD4^{+} and CD8^{+} populations in spleen from wild-type and T/NIX$^{-/-}$ mice. **(F)** Mean percentage of CD8^{+} (left) and CD4^{+} populations (right) from the experiment in panel **(E)**. **(G)** Representative dot plot showing percentage of CD8^{+} Naive (CD62L^{+}CD44^{-}), CD8^{+} central memory (CD62L^{+}CD44^{+}) and CD8^{+} effector (CD62L^{-}CD44^{+}) T cells in spleen from wild-type and T/NIX$^{-/-}$ mice. **(H)** Mean percentages of naïve CD8^{+} populations (left), total central memory (middle) and total effector CD8^{+} populations (right) from the corresponding gates in panel **(G)**. Data are representative of 2 independent experiments (n=4-8). Data were analyzed by two-tailed student's t-test (mean±SEM). ns= statistically not significant.

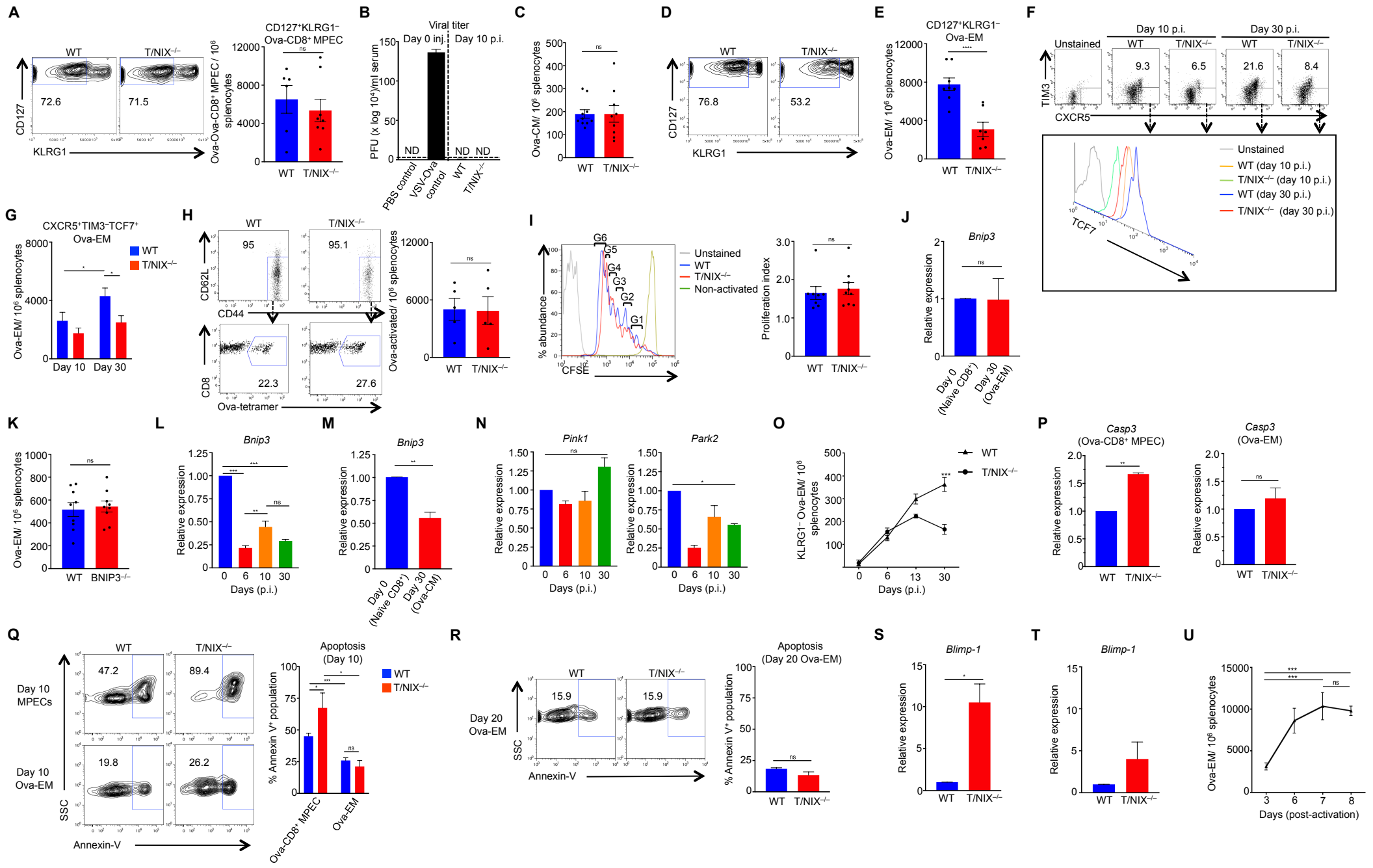
A
WT
T/NIX−/−
CD127
KLRG1
72.6
71.5
CD127+KLRG1−
Ova-CD8+ MPEC
Ova-Ova-CD8+ MPEC / 10^6 splenocytes
ns
B
Viral titer
Day 0 inj.
Day 10 p.i.
PFU (x log 10^4)/ml serum
ND
PBS control
VSV-Ova control
C
Ova-CM/ 10^6 splenocytes
D
76.8
53.2
E
CD127+KLRG1−
Ova-EM
Ova-EM/ 10^6 splenocytes
F
Unstained
Day 10 p.i.
Day 30 p.i.
9.3
6.5
21.6
8.4
TIM3
CXCR5
TCF7
Unstained
WT (day 10 p.i.)
T/NIX−/− (day 10 p.i.)
WT (day 30 p.i.)
T/NIX−/− (day 30 p.i.)
G
CXCR5+TIM3−TCF7+
Ova-EM
Ova-EM/ 10^6 splenocytes
Day 10
Day 30
H
95
95.1
CD62L
CD44
CD8
22.3
27.6
Ova-tetramer
Ova-activated/ 10^6 splenocytes
I
G6
G5
G4
G3
G2
G1
% abundance
CFSE
Unstained
WT
T/NIX−/−
Non-activated
Proliferation index
J
Bnip3
Relative expression
Day 0 (Naive CD8+)
Day 30 (Ova-EM)
K
Ova-EM/ 10^6 splenocytes
BNIP3−/−
L
Bnip3
Relative expression
Days (p.i.)
M
Bnip3
Day 0 (Naive CD8+)
Day 30 (Ova-CM)
N
Pink1
Park2
Days (p.i.)
O
KLRG1− Ova-EM/ 10^6 splenocytes
Days (p.i.)
P
Casp3
(Ova-CD8+ MPEC)
Casp3
(Ova-EM)
Q
Day 10 MPECs
Day 10 Ova-EM
47.2
89.4
19.8
26.2
SSC
Annexin-V
Apoptosis
(Day 10)
% Annexin V+ population
Ova-CD8+ MPEC
Ova-EM
R
Day 20 Ova-EM
15.9
15.9
Apoptosis
(Day 20 Ova-EM)
S
Blimp-1
T
Blimp-1
U
Ova-EM/ 10^6 splenocytes
Days (post-activation)

Figure S2. Characterization of CD8$^+$ T Cell Memory Formation in Wild-type and T/NIX$^{-/-}$ Mice, Related to Figure 1. (A) Left: Representative contour plot showing frequency of CD127$^+$KLRG1$^-$ CD8$^+$ Ova-specific memory precursor effector cells (CD127$^+$KLRG1$^-$ Ova-CD8$^+$ MPEC) in the spleen of OT-I wild-type or OT-I T/NIX$^{-/-}$ mice 10 days after VSV-Ova immunization. Right: Mean frequency of CD127$^+$KLRG1$^-$ Ova- CD8$^+$ MPEC from the left panel. **(B)** Serum viral titer in WT or T/NIX-$^{-/-}$ mice on 0 or 10 days after immunization with 10^4 PFU of VSV-Ova. **(C)** Mean frequency of Ova-specific central memory CD8$^+$ T cells (Ova-CM) in spleen of wild-type or T/NIX$^{-/-}$ mice 30 days after VSV-Ova immunization. **(D)** Representative contour plot showing frequency of CD127$^+$KLRG1$^-$ Ova-specific effector memory CD8$^+$ T cells (CD127$^+$KLRG1$^-$ Ova-EM) in the spleen of OT-I wild-type or OT-I T/NIX$^{-/-}$ mice 30 days after VSV-Ova immunization. **(E)** Mean frequency of CD127$^+$KLRG1$^-$ Ova-EM from panel **(D)**. **(F)** Representative FACS plot showing FACS staining for TIM3, CXCR5 and TCF7 in Ova-EM harvested from the spleens of OT-I wild-type or OT-I T/NIX$^{-/-}$ mice after VSV-Ova immunization. TIM3$^-$CXCR5$^+$ Ova-EM populations were further sub-gated into TCF7$^+$ population and TIM3$^-$CXCR5$^+$TCF7$^+$ population represented TIM3$^-$CXCR5$^+$TCF7$^+$Ova-EM. **(G)** Mean frequency of TIM3$^-$CXCR5$^+$TCF7$^+$ Ova-EM from panel **(F)**. **(H)** Left: Representative dot plot showing the percentage of Ova-specific activated CD8$^+$ T cells (Ova-activated) in the spleens of wild-type or T/NIX$^{-/-}$ mice 6 days after VSV-Ova immunization. Right: Mean frequencies of Ova-specific activated CD8$^+$ T cells from the left panel. **(I)** Left: Representative histogram showing proliferation of CD8$^+$ T cells (from unimmunized WT or T/NIX$^{-/-}$ spleens) activated *in vitro* with 1ug/mL of anti-mouse CD3 and CD28 antibodies. Peaks corresponding to G1, G2, G3, G4, G5 and G6 represent the generations of cells after successive cell division cycles. Right: Proliferation index of CFSE-stained CD8$^+$ T cells from the left panel. CFSE staining was measured 3 days after activation. **(J)** Gene expression of *Bnip3* in naïve CD8$^+$ T cells before and in Ova-EM 30 days after VSV-Ova immunization. Ova-EM from mice within the same experimental group were pooled before analysis. **(K)** Mean frequencies of Ova-specific effector memory CD8$^+$ T cells (Ova-EM) in spleen of wild-type or BNIP3$^{-/-}$ mice 30 days after VSV-Ova immunization. **(L)** Kinetics of *Bnip3* expression in Ova-specific CD8$^+$ T cells in OT-I mice at designated time points after immunization with VSV-Ova. **(M)** Gene expression of *Bnip3* in naïve CD8$^+$ T cells before and Ova-CM 30 days after VSV-Ova immunization. Naïve and Ova-CM from mice within the same experimental group were pooled before analysis. **(N)** Kinetics of *Pink1 and Park2* expression in Ova-specific CD8$^+$ T cells in OT-I mice at designated time points after immunization with VSV-Ova. **(O)** Time course experiment showing the kinetics of formation of KLRG1$^-$ Ova-specific effector memory CD8$^+$ T cells *in vivo* in wild-type or T/NIX$^{-/-}$ mice. **(P)** Gene expression of *Caspase-3 (Casp3)* in day 10 Ova-CD8$^+$ MPEC (*left*) and day 20 Ova-EM (*right*) harvested from WT and T/NIX$^{-/-}$ mice after VSV-Ova immunization. Apoptosis in **(Q)** day 10 Ova-CD8$^+$ MPEC or day 10 Ova-EM and **(R)** day 20 Ova-EM in WT or T/NIX$^{-/-}$ mice after VSV-Ova immunization, as indicated by percentage of annexin V$^+$ populations. Ova-CD8$^+$ MPEC or Ova-EM from WT or T/NIX$^{-/-}$ mice were further sub-gated into Annexin V$^+$ population. Gene expression of *Blimp-1* in **(S)** Ova-CD8$^+$ MPEC and **(T)** Ova-EM harvested from VSV-Ova immunized WT and T/NIX$^{-/-}$ mice. Ova-CD8$^+$ MPEC in **(S)** and Ova-EM in **(T)** from mice within the same experimental group were pooled before analysis. **(U)** Kinetics of *in vitro* formation of effector memory in wild-type CD8$^+$ T cells. Splenocytes from WT mice were activated with 50ug/mL Ovalbumin in presence of 100 units/mL IL-2 for 3 days, after which cells were washed and fresh IL-15 added on the same day. Data in **(A, C-K, M, O, S-U)** are representative of $\geq$2 independent experiments (n=5-11) and data in **(B, L, N, P-R)** are representative of 3-10 biological replicates/group. Data in **(A)**, **(C)**, **(E)**, **(H)**, **(I)**, **(J)**, **(K)**, **(M)**, **(P)**, **(Q)**, **(R)**, **(S)** and **(T)** were analyzed by two-tailed student's t-test (mean$\pm$SEM), data in **(G)**, **(L), (N)** and **(U)** were analyzed by One-way ANOVA with Bonferroni's posttests (mean$\pm$SEM) and data in **(O)** were analyzed by Two-way ANOVA with Bonferroni's posttests (mean$\pm$SEM). **** $p<0.0001$, *** $p<0.001$, ** $p< 0.01$, * $p<0.05$, ns= non-significant.

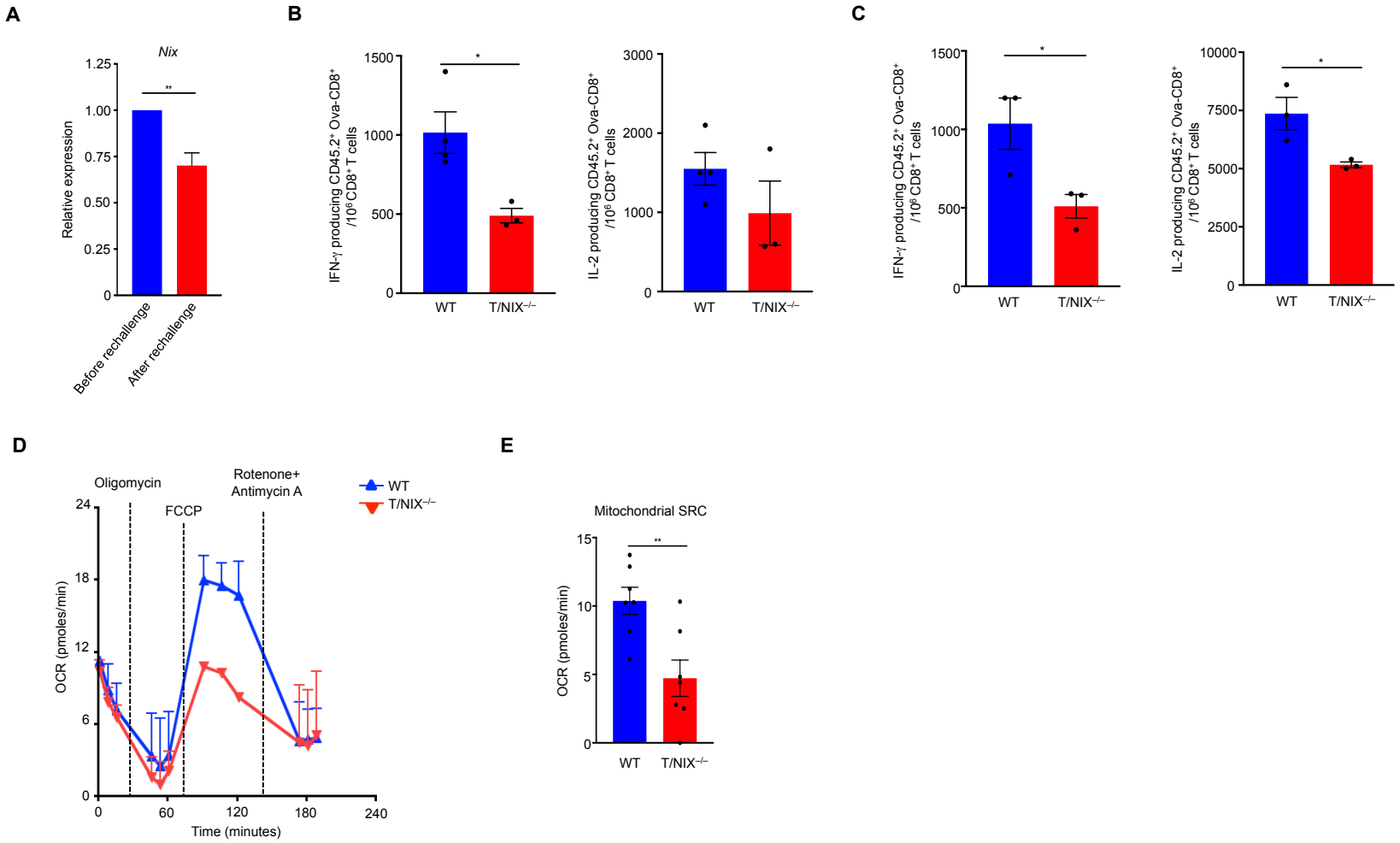

Figure S3. Characterization of memory recall by Wild-type and T/NIX$^{-/-}$ Ova-Specific Effector Memory CD8$^+$ T cells, Related to Figure 2. Ova-specific effector memory CD8$^+$ T cells formed *in vivo* **(A, B)** or *in vitro* **(C)** from CD45.2$^+$ mice (OT-I wild-type and OT-I T/NIX$^{-/-}$) were adoptively transferred intravenously into naïve CD45.1$^+$ mice. CD45.1$^+$ host were then challenged with 10^4 PFU of VSV-Ova 24 hours later. 48 hours after VSV-Ova challenge, host CD45.1$^+$ mice were sacrificed and Ova-EM were sorted from their splenocytes for further experiments. **(A)** Gene expression of *Nix* in WT Ova-EM before and after VSV-Ova rechallenge. Data points are represented relative to *Nix* expression before rechallenege. **(B)** Mean frequencies of IFN- γ (left) and IL-2 (right) producing CD45.2$^+$ Ova-specific CD8$^+$ T cells from **figure 2C**. **(C)** Mean frequencies of IFN- γ (left) and IL-2 (right) producing CD45.2$^+$ Ova-specific CD8$^+$ T cells from **figure 2H. (D)** Representative Oxygen Consumption rate (OCR) in Ova-specific effector memory CD8$^+$ T cells formed *in vitro* (OT-I wild-type or OT-I T/NIX$^{-/-}$ cells). **(E)** Mitochondrial spare respiratory capacity (SRC) from experiment in **(D)**. Data in (**A-C**) are representative of 3-4 biological replicates/group and data in **(D, E)** are representative of $\geq$2 independent experiments (n=7). Data in **(A), (B), (C)** and **(E)** were analyzed by two-tailed student's t-test (mean$\pm$SEM). ** $p<0.01$, *$p<0.05$.

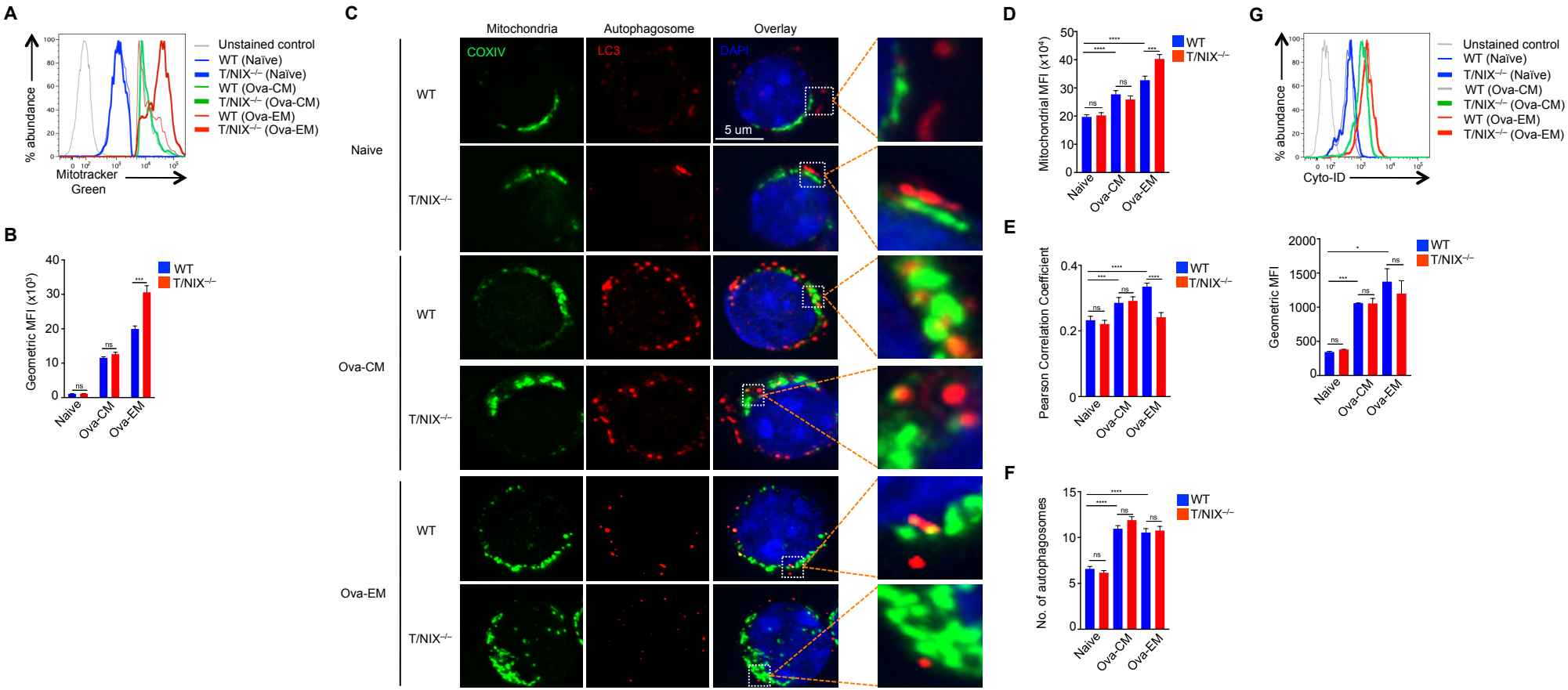

Figure S4. Characterization of Mitophagy in Naïve, Effector Memory and Central Memory CD8⁺ T Cells from Wild-type and T/NIX$^{-/-}$ Mice, Related to Figure 3. (A) Representative histogram showing Mitotracker Green staining in naïve, Ova-specific effector memory (Ova-EM) and Ova-specific central memory (Ova-CM) CD8⁺ T cells from wild-type and T/NIX$^{-/-}$ mice. **(B)** MFI for total mitochondrial mass from the experiment in panel **(A)**. **(C)** Representative deconvolution microscopic image of naïve, Ova-EM and Ova-CM stained with COX IV (mitochondria) and LC3 (autophagosomes). **(D)** Mitochondrial median fluorescence index (mitochondrial MFI), **(E)** mitochondrial autophagy and **(F)** number of autophagosome punctate in naïve, Ova-EM and Ova-CM populations from the experiment in panel **(C)**. **(G)** Top: Representative Cyto-ID staining showing autophagy flux in naïve, Ova-EM and Ova-CM 30 days after VSV-Ova immunization. Bottom: Mean geometric MFI of Cyto-ID staining from experiment in top panel. For each independent experiment in panels **(C-G)**, spleens were harvested from WT or T/NIX$^{-/-}$ mice and sorted for respective populations. Sorted cells were pooled from within the same experimental group before further analysis. For each independent experiment in panels **(D-F)**, ~100-200 cells/group were quantified. Data are representative of $\geq$2 independent experiments (n=4-5). Data were analyzed by two-tailed student's t-test (mean $\pm$SEM). **** $p<0.0001$, *** $p<0.001$, * $p<0.05$, ns= non-significant.

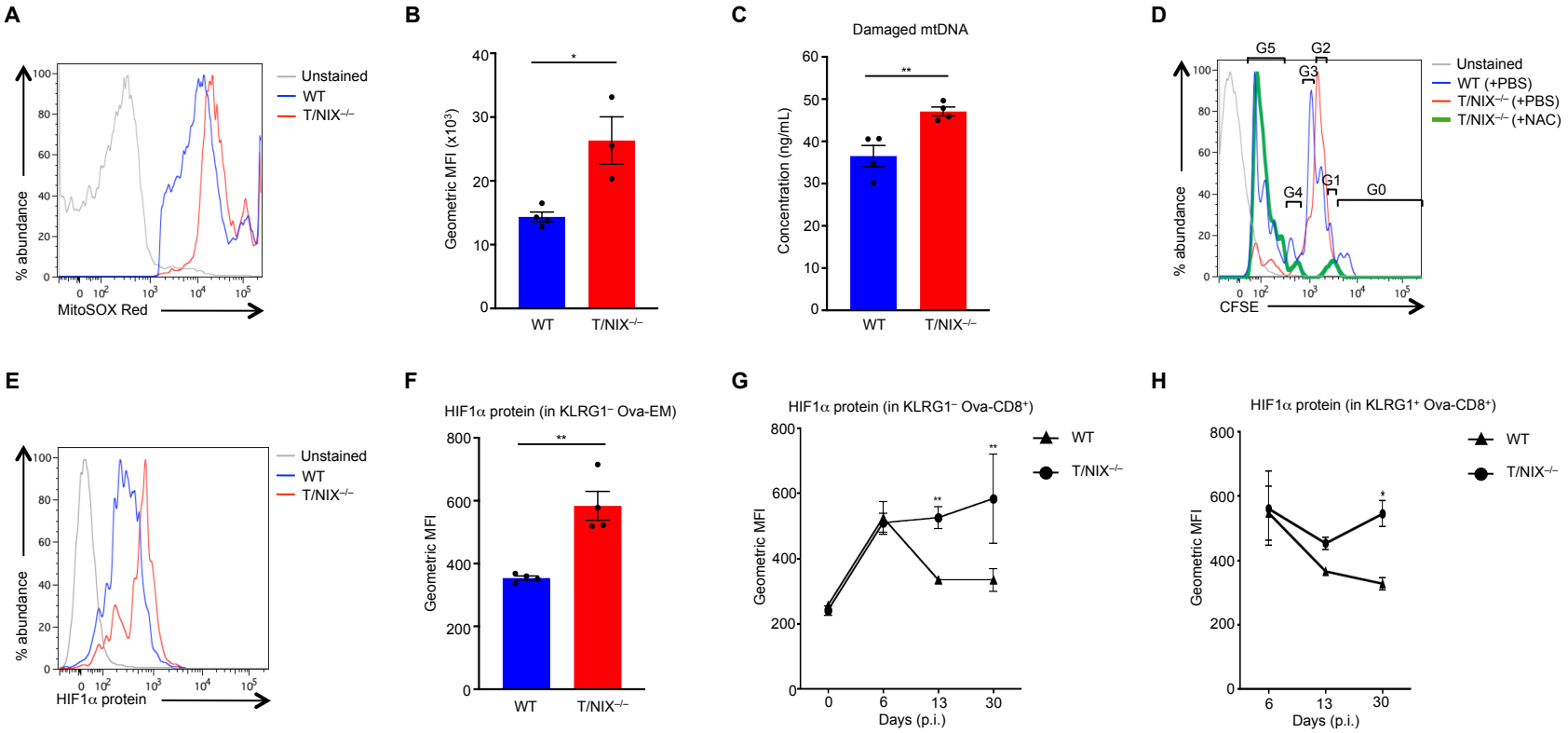

Figure S5. Characterization of mitochondrial superoxide, memory recall and HIF1α in Antigen-specific Effector Memory CD8⁺ T Cells from Wild-type and T/NIX$^{-/-}$ Mice, Related to Figures 4 and 5. (A) Representative histogram showing MitoSOX Red staining in Ova-specific CD8⁺ T cells from wild-type and T/NIX$^{-/-}$ mice 10 days after immunization. **(B)** Geometric mean fluorescence index for mitochondrial superoxide in Ova-specific CD8⁺ T cells from experiments performed in panel **(A)**. **(C)** Level of damaged mitochondrial DNA in Ova-specific CD8⁺ T cells from OT-I wild-type and OT-I T/NIX$^{-/-}$ mice 20 days after immunization. **(D)** *In vivo* proliferation of wild-type or T/NIX$^{-/-}$ Ova-specific effector memory CD8⁺ T cells (formed *in vivo* in presence of vehicle or NAC) measured by CFSE staining. Ova-specific effector memory CD8+ T cells were labelled with CFSE before adoptive transfer into CD45.1⁺ recipients, with subsequent VSV-Ova re-challenge. Peaks corresponding to G1, G2, G3, G4 and G5 represent the generations of cells after successive cell division cycles. Proliferation index for WT (+PBS), T/NIX$^{-/-}$ (+PBS) and T/NIX$^{-/-}$ (+NAC) are 2.37±0.067, 2.07±0.067 and 3.67±0.37 respectively. Proliferation index was found to be significantly different between WT (+PBS) and T/NIX$^{-/-}$ (+PBS) ($p<0.05$) and between T/NIX$^{-/-}$ (+PBS) and T/NIX$^{-/-}$ (+NAC) ($p<0.05$). **(E)** Representative histogram showing intracellular HIF1α protein level in KLRG1⁻ population of Ova-specific effector memory CD8⁺ T cells 30 days after VSV-Ova immunization in wild-type and T/NIX$^{-/-}$ mice. **(F)** MFI of HIF1α protein staining in KLRG1⁻ population of Ova-specific effector memory CD8⁺ T cells from experiment performed in panel **(E)**. MFI of intracellular HIF1α protein level in **(G)** KLRG1⁻ Ova-specific effector CD8⁺ T cells, and **(H)** KLRG1⁺ Ova-specific effector CD8⁺ T cells on indicated time points after VSV-Ova immunization in wild-type and T/NIX$^{-/-}$ mice. Data in **(A-C)** are representative of 3-5 biological replicates/group and data in **(D-H)** are representative of 2 independent (n=3-6). Data in **(B)**, **(C)**, **(D)** and **(F)** were analyzed by two-tailed student's t-test (mean±SEM) and data in **(G)** and **(H)** were analyzed by two-way ANOVA with Bonferroni's post-tests (mean ±SEM). *** $p<0.001$, ** $p<0.01$, * $p<0.05$, ns= non-significant.

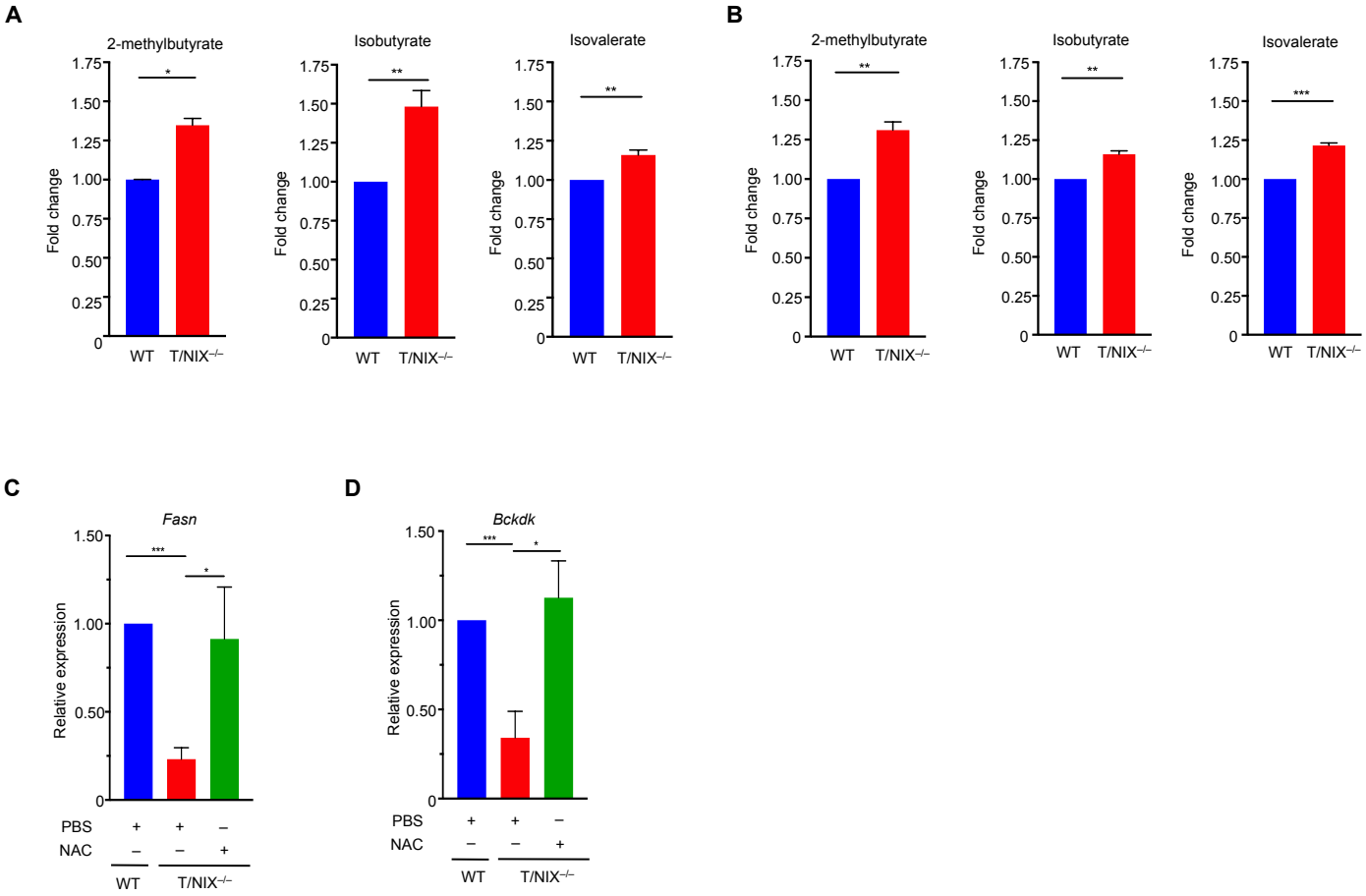

Figure S6. Characterization of fatty acid metabolism in Antigen-specific Effector Memory CD8⁺ T Cells from Wild-type and T/NIX$^{-/-}$ Mice, Related to Figure 6. For each independent experiment, cells were sorted from WT or T/NIX$^{-/-}$ mice 30 days after VSV-Ova-immunization(10^4 PFU/mouse) and pooled from within the same experimental group before further analysis. Fold change in short/branched-chain fatty acids in **(A)** Ova-specific CD8$^+$ MPECs, and **(B)** Ova-specific memory CD8$^+$ T cells formed *in vivo* in OT-I wild-type or OT-I T/NIX$^{-/-}$ mice. Gene expression of **(C)** *Fasn* and **(D)** *Bckdk* in Ova-specific effector memory CD8$^+$ T cells in wild-type and T/NIX$^{-/-}$ mice (vehicle or NAC-treated). Data are representative of 2 independent experiments (n=4-7). Data were analyzed by two-tailed student's t-test (mean$\pm$SEM). *** $p<0.001$, ** $p<0.01$, * $p<0.05$, ns= non-significant.

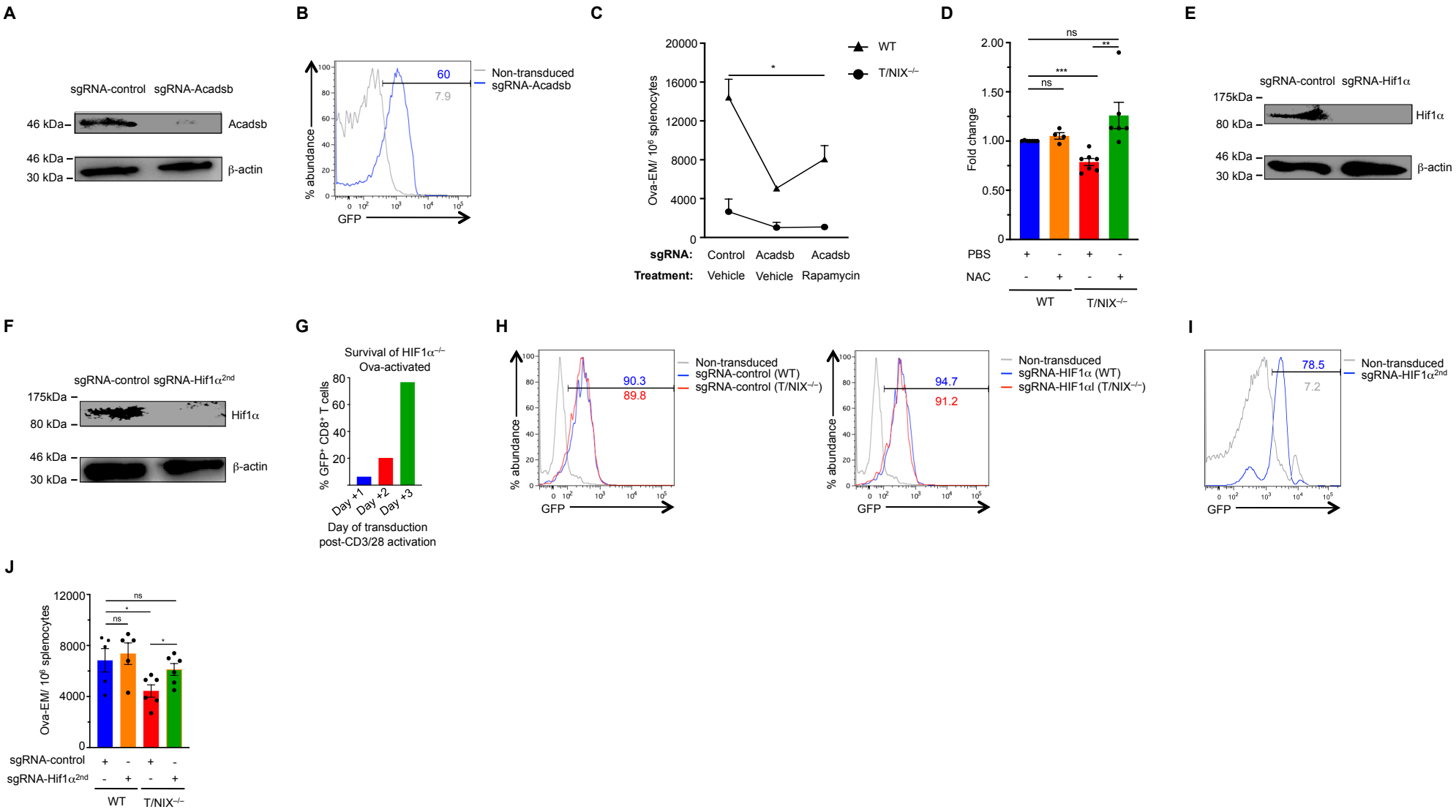
A
sgRNA-control sgRNA-Acadsb
46 kDa
Acadsb
46 kDa
30 kDa
β-actin
B
% abundance
GFP
60
7.9
Non-transduced
sgRNA-Acadsb
C
Ova-EM/ 10^6 splenocytes
WT
T/NIX−/−
sgRNA: Control Acadsb Acadsb
Treatment: Vehicle Vehicle Rapamycin
D
Fold change
ns
**
***
ns
PBS
NAC
WT
T/NIX−/−
E
sgRNA-control sgRNA-Hif1α
175kDa
80 kDa
Hif1α
46 kDa
30 kDa
β-actin
F
sgRNA-control sgRNA-Hif1α2nd
175kDa
80 kDa
Hif1α
46 kDa
30 kDa
β-actin
G
Survival of HIF1α−/− Ova-activated
% GFP+ CD8+ T cells
Day +1
Day +2
Day +3
Day of transduction post-CD3/28 activation
H
% abundance
GFP
90.3
89.8
Non-transduced
sgRNA-control (WT)
sgRNA-control (T/NIX−/−)
94.7
91.2
Non-transduced
sgRNA-HIF1α (WT)
sgRNA-HIF1αl (T/NIX−/−)
I
78.5
7.2
Non-transduced
sgRNA-HIF1α2nd
GFP
J
Ova-EM/ 10^6 splenocytes
ns
*
ns
*
sgRNA-control
sgRNA-Hif1α2nd
WT
T/NIX−/−

Figure S7. Characterization of Effector Memory Formation in HIF1$\alpha^{-/-}$ or ACADSB$^{-/-}$ CD8^{+} T Cells Using CRISPR/Cas9-mediated Genome Editing, Related to Figures 6 and 7. (A) Western blot of ACADSB protein in Ova-specific CD8^{+} T cells after transduction with LentiCRISPRv2 expressing sgRNA-control or sgRNA-ACADSB. **(B)** Representative histogram plot showing percentage GFP expression in Ova-specific CD8^{+} T cells post-transduction with LentiCRISPRv2 (sgRNA-ACADSB). Percentage GFP expression represents percent transduction of LentiCRISPRv2. **(C)** Effect of rapamycin treatment on effector memory formation in ACADSB$^{-/-}$ CD8^{+} T cells. **(D)** Intracellular ATP in Ova-specific effector memory CD8^{+} T cells 30 days after VSV-Ova immunization in wild-type and T/NIX$^{-/-}$ mice (treated with vehicle control or NAC). For each independent experiment, Ova-specific effector memory CD8^{+} T cells were pooled from all the mice within the same experimental group and ATP was measured in the cells. Each point represents an individual independent experiment. Western blot of HIF1α protein in Ova-specific CD8^{+} T cells after transduction with **(E)** LentiCRISPRv2 expressing sgRNA-control or sgRNA-HIF1α, and **(F)** LentiCRISPRv2 expressing sgRNA-control or sgRNA-HIF1α^{2nd}. **(G)** Mean frequencies of Ova-specific CD8^{+} T cells transduced with LentiCRISPRv2 (sgRNA-HIF1α) at different time points after activation with anti-CD3 and anti-CD28 antibodies. Representative histogram plot showing percentage GFP expression in Ova-specific CD8^{+} T cells post-transduction with **(H)** LentiCRISPRv2 (sgRNA-control or sgRNA-HIF1α) and **(I)** LentiCRISPRv2 (sgRNA-HIF1α^{2nd}). Percentage GFP expression represents percent transduction of LentiCRISPRv2. **(J)** Effect of loss of HIF1α on effector memory formation. OT-I wild-type or OT-I T/NIX$^{-/-}$ cells were transduced with LentiCRISPRv2 expressing sgRNA-control or sgRNA-HIF1α^{2nd}. Immunoblots in panels **A, E** and **F** were cropped to include only the relevant groups. Brightness, contrast, color balance and sharpness in panels **A, E** and **F** were applied to the entire image corresponding to any immunoblot. Data in **(C)** are representative of 3-4 biological replicates/group and data in **(D, J) a**re representative of $\geq$2 independent experiments (n=4-7**)**. Data in **(C), (D)** and **(J)** were analyzed by two-tailed student's t-test (mean$\pm$SEM). *** $p<0.001$, ** $p<0.01$, * $p<0.05$, ns= non-significant.

Table S1. Primer and sgRNA sequences, Related to STAR methods.

Primer/sgRNA	Sequence
Primer: *18S* forward	ATTGACGGAAGGGCACCAC
Primer: *18S* reverse	TCTAAGAAGTTGGGGGACGC
Primer: *Nix* forward	GAGCCGGATACTGTCGTCCT
Primer: *Nix* reverse	CAATATAGATGCCGAGCCCCA
Primer: *Bnip3* forward	AACAGCACTCTGTCTGAGGAA
Primer: *Bnip3* reverse	TGTCAGACGCCTTCCAATGT
Primer: *Il-15rα* forward	ACATCGGTCCTCTTGGTTGG
Primer: *Il-15rα* reverse	CGTGTGGTTAGGCTCCTGTG
Primer: *Foxo1* forward	CACACATCTGCCATGAACCG
Primer: *Foxo1* reverse	GGTGGAGGACACCCATCCTA
Primer: *Tcf7* forward	CGGAAAGAAGAAGAGGCGGT
Primer: *Tcf7* reverse	CTGTCATCGGAAGGAACGGG
Primer: *Blimp-1* forward	GGACTGGGTGGACATGAGAG
Primer: *Blimp-1* reverse	TTCACGTAGCGCATCCAGTT
Primer: *Tfam* forward	TAGGCACCGTATTGCGTGAG
Primer: *Tfam* reverse	GACAAGACTGATAGACGAGG GG
Primer: *Fasn* forward	TTGACGGCTCACACACCTAC
Primer: *Fasn* reverse	TTGTGGTAGAAGGACACGGC
Primer: *Bckdk* forward	TTCCCCTTCATTCCCATGCC
Primer: *Bckdk* reverse	CCGTAGGTAGACATCCGTGC
Primer: *Acadl* forward	GTGTATCGGTGCCATAGCCA
Primer: *Acadl* reverse	AGGCAGAAATCGCCAACTCA
Primer: *Acadsb* forward	GAAAAATGCCCGAGGCTCAC
Primer: *Acadsb* reverse	TGCATCCACCCCTTCCTTTC
Primer: *Acadm* forward	TTCGAAGACGTCAGAGTGCC
Primer: *Acadm* reverse	GCTCCACTAGCAGCTTTCCA
Primer: *Acads* forward	TTGCCGAGAAGGAGTTGGTC
Primer: *Acads* reverse	AGGTAATCCAAGCCTGCACC
Primer: *Acad11* forward	CGCCTTGGACCTGGAAGAAT
Primer: *Acad11* reverse	TTCAAGGTCAGCAAGCGGAT
Primer: *Atp5b* forward	GTTGGTCCTGAGACCTTGGG
Primer: *Atp5b* reverse	TCCGATTTTCCCACCCTTGG
Primer: *Atp5f1* forward	TCCAGGGGTATTACAGGCAAC
Primer: *Atp5f1* reverse	CAGCCCAAGACGCACTTTTC
Primer: *Ehhadh* forward	CGGTCAATGCCATCAGTCCA
Primer: *Ehhadh* reverse	AGCACCTGCACAGAAGTTGT
Primer: *Gls* forward	CCGCGGGCGACAATAAAATA A
Primer: *Gls* reverse	GCATGACACCATCTGACGTT
Primer: *Glut1* forward	ATAGTTACAGCGCGTCCGTT
Primer: *Glut1* reverse	AGAGACCAAAGCGTGGTGAG
Primer: *Prkaa1* forward	GTGAAGATCGGCCACTACATC C
Primer: *Prkaa1* reverse	GGCTTTCCTTTTCGTCCAACC

Primer: *Pdha1* forward	GCCACCCTGAACCTGAGAAA
Primer: *Pdha1* reverse	GCGATACATCATTACATCCACG
Primer: *Pink1* forward	GTGGGACTCAGATGGCTGTC
Primer: *Pink1* reverse	GCACATTTGCAGCTAAGCGT
Primer: *Parkin* forward	CCAAACCGGATGAGTGGTGAGTGC
Primer: *Parkin* reverse	ACACGGCAGGGAGTAGCCAAGTTG
Primer: *Caspase-3* forward	AGCTGGACTGTGGCATTGAG
Primer: *Caspase-3* reverse	CCACGACCCGTCCTTTGAAT
sgRNA targeting sequence: *Hif1α* forward	CACCGTGATAACGTGAACAAATACA
sgRNA targeting sequence: *Hif1α* reverse	AAACTGTATTTGTTCACGTTATCAC
sgRNA targeting sequence: *Hif1α* forward^{2nd}	CACCGAAGCATCCTGTACTGTCCTG
sgRNA targeting sequence: *Hif1α* reverse^{2nd}	AAACCAGGACAGTACAGGATGCTTC
sgRNA targeting sequence: *Acadsb* forward	CACCGATGGATGAGAACTCAAAAA
sgRNA targeting sequence: *Acadsb* reverse	AAACTTTTTGAGTTCTCATCCATC